

1 **The last interglacial (Eemian) climate simulated by LOVECLIM and CCSM3**

2

3 **Irina Nikolova^{1*}, Qiuzhen Yin¹, Andre Berger¹, Umesh Kumar Singh¹ and Mehdi Pasha**
4 **Karami¹**

5

6 1 George Lemaitre Centre for Earth and Climate Research, Earth and Life Institute, Universite
7 Catholique de Louvain, 3, Place Louis Pasteur, 1348 Louvain-la-Neuve, Belgium

8 * corresponding author: e-mail: irina.nikolova@uclouvain.be

9

10 **Abstract**

11

12 This paper presents a detailed analysis of the climate of the last interglacial simulated by two
13 climate models of different complexities, CCSM3 and LOVECLIM. The simulated surface
14 temperature, hydrological cycle, vegetation and ENSO variability during the last interglacial
15 are analyzed through the comparison with the simulated Pre-Industrial (PI) climate. In both
16 models, the last interglacial period is characterized by a significant warming (cooling) over
17 almost all the continents during boreal summer (winter) leading to a largely increased
18 (reduced) seasonal contrast in the northern (southern) hemisphere. This is mainly due to the
19 much higher (lower) insolation received by the whole Earth in boreal summer (winter) during
20 this interglacial. The arctic is warmer than PI through the whole year, resulting from its much
21 higher summer insolation, its remnant effect in the following fall-winter through the interactions
22 between atmosphere, ocean and sea ice and feedbacks from sea ice and snow cover.
23 Discrepancies exist in the sea-ice formation zones between the two models. Cooling is
24 simulated by CCSM3 in the Greenland-Norwegian Seas and near the shelves of Antarctica
25 during DJF but not in LOVECLIM as a result of excessive sea-ice formation. Intensified
26 African monsoon is responsible for the cooling during summer in North Africa and on the
27 Arabian Peninsula. Over India precipitation maximum is found further west, while in Africa the
28 precipitation maximum migrates further north. Trees and grassland expand north in
29 Sahel/Sahara, more clearly seen in LOVECLIM than in CCSM3 results. A mix of forest and
30 grassland occupies continents and expand deep in the high northern latitudes. Desert areas

1 reduce significantly in Northern Hemisphere, but increase in North Australia. The interannual
2 SST variability of the tropical Pacific (El-Nino Southern Oscillation) of the last interglacial
3 simulated by CCSM3 shows slightly larger variability and magnitude compared to the PI.
4 However, the SST variability in our LOVECLIM simulations is particularly small due to the
5 overestimated thermocline's depth.

6

7 Keywords: Last interglacial, paleoclimate modeling, surface temperature, monsoon,
8 vegetation, ENSO

9

10 **1. Introduction**

11

12 The Earth has experienced quite warm periods in the past (e.g. interglacials). Investigating
13 the climate processes and feedbacks during these warm periods helps to improve our
14 understanding of climate dynamics and to address key questions for the future, in particular
15 when the climate predicted to occur over the next centuries by the Intergovernmental Panel
16 on Climate Change (IPCC, 2007) appears to be unprecedented over the last 150 years. The
17 last interglacial (also called the Eemian interglacial and Marine Isotope Stage (MIS) 5e) was a
18 recent warm interglacial during which the Arctic experienced markedly summer warming,
19 accompanied by sea-level rise and reduction in ice sheets (Otto-Bliesner et al., 2006a; Kukla
20 et al., 2002; Bintanja et al., 2005; Jouzel et al., 2007; McKay et al., 2011). In terms of such
21 climatic features, the last interglacial is often considered to be analogue to the future climate
22 (eg. Kukla et al., 1997), though this is still questionable in terms of its completely different
23 astronomical configuration from today and the future (Berger and Loutre, 1996; Berger and
24 Yin, 2012). There are still no detailed datasets compiled for MIS-5e except for the global
25 temperature record of Turney and Jones (2010). This is related to the fact that creating a
26 database based on individual records is complicated (Groll et al., 2005) due to the large
27 uncertainties related to difficulties in estimating the duration of MIS-5e (Shackleton et al.
28 2003). Given its significance in helping to understand better the future warming, the last
29 interglacial has been included recently in the Palaeoclimate Model Intercomparison project (in
30 its third phase, PMIP3, <http://pmip3.lsce.ipsl.fr>).

1
2 Yin and Berger (2010, 2012) have simulated the peak climates of the past nine interglacials
3 with LOVECLIM, an Earth system model of intermediate complexity. Using the same
4 boundary conditions, Herold et al. (2012) simulated the climate of five stronger interglacials
5 with CCSM3, a comprehensive Atmosphere-Ocean General Circulation Model. These studies
6 focused on the comparison between different interglacials. Because they used the same
7 climate forcings, these studies provide ideal paired experiments for inter-model comparison,
8 which would be interesting for the modeling community in particular given that LOVECLIM
9 and CCSM3 are often used in climate/paleoclimate modeling and are of different complexity.
10 The MIS-5e simulations provided by these studies and also included in Lunt et al (same
11 issue), are analyzed here. Lunt et al. (same issue) analyzed 18 snapshot simulations between
12 125ka and 130ka BP performed by several climate models. They focus on the analysis of
13 near surface temperature pointing out large regional deviations in the ensemble mean and
14 between ensemble mean and proxy data. However, due to the large amount of models, it is
15 difficult to address in details the possible reasons for the simulated regional dissimilarities
16 between the models. Given the increasing interest of the paleoclimate community in the last
17 interglacial climate, detailed information about the simulated climates is needed and the
18 mechanisms responsible for the changes of different climatic variables deserve to be
19 investigated. In this paper, we present a detailed regional and seasonal analysis for the
20 surface climates of MIS-5e relative to the Pre-Industrial (PI) period. We investigate the
21 feedbacks of sea ice, monsoon, vegetation and ENSO in the modeled climate system as
22 plausible explanations for the regional similarities/dissimilarities simulated in both models,
23 making it the first detailed intercomparison between CCSM3 and LOVECLIM models with
24 emphasis on MIS-5e. We also give some quantitative comparison with proxy data reported in
25 literature, in order to determine where features are robust and where uncertainties are large.

26
27 The paper is organized as follows: in Section 2 we give a brief description of CCSM3 and
28 LOVECLIM models and the prescribed boundary conditions. In Section 3 we discuss the
29 similarities and differences in surface temperature between CCSM3 and LOVECLIM. In
30 Section 4 we focus on African, Indian and East Asian monsoons. Vegetation is discussed in

1 Section 5 and ENSO variability in Section 6. Conclusions are given in Section 7.

2

3 **2. Model descriptions**

4

5 **2.1. CCSM3 and BIOME4**

6

7 The Community Climate System Model 3 (CCSM3) is a coupled climate model with
8 components representing the atmosphere, ocean, sea ice and land surface connected by a
9 flux coupler (Collins et al., 2006). The atmospheric model is CAM3 (Collins et al., 2004).
10 CAM3 has 26 vertical levels and a 3.75°x3.75° horizontal resolution which corresponds to T31
11 configuration. The land model CLM version 3.0 (Oleson et al. 2004) is integrated on the same
12 horizontal grid as the atmosphere, with each grid box further divided into a hierarchy of land
13 units and soil columns. The ocean model POP (Smith and Gent, 2002) uses a dipole grid with
14 a horizontal resolution of 3°x1.5° in longitude and latitude, respectively. Vertically, the model
15 has 25 levels that extend to 4.75km. The sea-ice model CSIM (Briegleb et al., 2004) is a
16 dynamical model and has the same horizontal resolution as the ocean model POP. Ice sheets
17 are prescribed as today. In the CCSM3 model framework there is no dynamically coupled
18 vegetation module. Instead, vegetation is estimated using the offline vegetation model
19 BIOME4 (Kaplan et al., 2003). CCSM3 output variables (such as temperature, precipitation,
20 cloudiness, etc.) are used to force the BIOME4, to see what would be the vegetation
21 distribution given the simulated climate. BIOME4 has 28 types of plants which we grouped
22 into 3 major categories – a) forest that includes the following vegetation: tropical evergreen
23 forest, tropical semi-deciduous forest, tropical deciduous forest/woodland, temperate
24 deciduous forest, temperate conifer forest, warm mixed forest, cool mixed forest, cool conifer
25 forest, cold mixed forest, evergreen taiga forest, deciduous taiga forest, tropical savanna,
26 temperate broadleaved savanna, open conifer woodland, temperate sclerophyll woodland; b)
27 grass that includes: tropical xerophytic shrubland, temperate xerophytic shrubland, tropical
28 grassland, temperate grassland, boreal parkland, steppe tundra, shrub tundra, dwarf shrub
29 tundra, prostrate shrub tundra, cushion-forbs, lichen and moss and c) desert that includes
30 desert, barren and land ice.

1
2
3
4
5
6
7
8
9
10
11
12
13
14
15
16
17
18
19
20
21
22
23
24
25
26
27
28
29
30

2.2. LOVECLIM

LOVECLIM is a three dimensional Earth system model of intermediate complexity (Goosse et al., 2010). The atmosphere model ECBilt is a quasi-geostrophic model with 3 vertical levels and $5.625^{\circ} \times 5.625^{\circ}$ (T21) horizontal resolution (Opsteegh et al., 1998). CLIO is a primitive-equation, free-surface ocean general circulation model coupled to a thermodynamic-dynamic sea ice model (Goosse and Fichefet, 1999). The horizontal resolution is $3^{\circ} \times 3^{\circ}$ and there are 20 levels on the vertical in the ocean. VECODE is the vegetation model, developed by Brovkin et al. (1997). Based on annual mean values of several climatic variables, the VECODE model computes the evolution of the vegetation cover described as a fractional distribution of desert, tree and grass in each land grid cell with the same resolution as that of ECBilt. In this study, the atmosphere, ocean-sea ice and vegetation are interactively coupled, and the ice sheets are prescribed as today.

2.3. Boundary conditions for the equilibrium experiments

In our experiments, MIS-5e has the astronomical configuration of 127 ka BP. It is worthy noting that several dates around the peak of the last interglacial have been used to select the insolation forcing in previous studies (see the summary in Lunt et al, same issue). According to the strategy of Yin and Berger (2010, 2012), insolation at 127 ka BP was used in our MIS-5e experiments of both LOVECLIM and CCSM3. This is because, following the hypothesis that an interglacial is associated with a strong summer insolation in Northern Hemisphere (NH), the insolation was taken at the dates when NH summer occurred at perihelion just preceding the interglacial peak taking into account a few thousands of years of lag between the forcing and climatic response. Compared to PI, MIS-5e climate is driven by much larger eccentricity (0.03937 vs. 0.01672 for PI) and obliquity (24.040° vs. 23.446° for PI) (Berger, 1978). NH summer occurring at perihelion, a situation opposite to PI, leads to much more insolation received on Earth during boreal summer (Figure 1). The CO₂ equivalent concentration (contribution of CO₂, CH₄ and N₂O) is taken to be 284 ppmv in MIS-5e and 280

1 ppmv in PI (Table 1). As a result, the differences observed between MIS-5e and PI climate are
2 mainly driven by the strong astronomically-induced seasonal forcing of MIS-5e.

3

4 In CCSM3, the Pre-Industrial climate is a 900-year continuation run from year 400 of the
5 simulation conducted at the National Center for Atmospheric Research (Otto-Bliesner et al.,
6 2006b). The MIS-5e simulation is initiated from PI simulation at year 500 and run for 1000
7 years. In LOVECLIM, the simulations of PI and MIS-5e are both 1000-year long equilibrium
8 run. The results of the last 100-year are used for analysis.

9

10 **3. Simulated surface temperature anomalies**

11

12 Compared to PI, the global annual mean surface temperature of MIS-5e is 0.5°C warmer in
13 LOVECLIM and 0.2°C cooler in CCSM3 (Table 2). Terrestrial and marine records indicate a
14 warming of about 1.9°C during MIS-5e relative to preindustrial (Turney and Jones, 2010)
15 which is underestimated by LOVECLIM and CCSM3. In addition to the possible uncertainty in
16 the estimation based on proxy records, one of the reasons might be due to the lack of
17 interactive ice sheets in both models. Holden et al. (2010) investigated the effect of warming
18 in Antarctica when accounting for dynamic ice sheets. They found that the surface
19 temperature in East Antarctica increased from 1.4 (Dome C) and 2.2°C (Dome F) to 5 (Dome
20 C) and 4.9°C (Dome F) caused by the retreat and meltwater of the West Antarctic Ice Sheet
21 (WAIS). In NH, according to Otto-Bliesner et al (2006a), when Greenland ice sheet is
22 completely removed, there is an additional summer warming of several to more than 10°C
23 localized over Greenland, and the freshwater forcing of inserting 0.1 sverdrup of water in the
24 North Atlantic over 100 years yields to an annual cooling of 1.5°C south of Greenland. In spite
25 of this fresh water induced cooling, the summer temperature anomalies over Greenland
26 remain positive. Lunt et al (2004) also found that the effect of melted Greenland is local for
27 temperature (directly related to changes in altitude and albedo of the surface), precipitation
28 and more widespread for circulation (response to changed orography) but the “principal effect
29 of removing the Greenland ice-sheet is relatively localised”. They show that December-
30 January-February (DJF) surface temperature decreases over Barents Sea (2°C for 2m height

1 temperature) as a result of changes in the near-surface meridional wind speed. In the case of
2 melted Greenland, cold air from the pole is advected to the south. This cooling along with the
3 freshening of the North Atlantic increases the sea-ice formation and retains sea ice in June-
4 July-August (JJA) as mentioned by Lunt et al (2004). However, all these sensitivity studies are
5 for a complete melting of Greenland ice sheet, therefore the effects of the MIS-5e Greenland
6 melting would be much smaller and would be important mainly for the regions over and
7 around Greenland. Nevertheless, the shortcoming of prescribing ice sheet to present should
8 be kept in mind when model-proxy comparison is made.

9
10 Global cooling is simulated in DJF and warming in JJA by both models. LOVECLIM simulates
11 consistently warmer climate than CCSM3. This might be related to the temperature biases in
12 both models and through feedbacks from the modeled climate system. Goosse et al (2010)
13 report that tropical regions in LOVECLIM are too warm and the temperature gradient between
14 the Eastern and Western Pacific is underestimated as a result of a warmer Eastern Pacific. In
15 CCSM3, Collins et al. (2006) report colder northern (60-90°N) and southern (60-90°S)
16 regions. Along with the missing feedback from dynamic ice sheets, the feedback from
17 vegetation could also affect the temperature through albedo change. As we discuss in Section
18 5, trees expanded deep into the northern high latitudes replacing grassland. The lack of
19 interactive vegetation in CCSM3 could cause unrealistic surface temperature because of the
20 missing response during the replacement. According to Brovkin (2002), climate exerts a major
21 control on the spatial distribution of vegetation types while vegetation influences climate via
22 changes in the physical properties of the land surface such as albedo, biogeophysical
23 mechanisms, roughness and atmospheric gas composition. For example Crucifix and Loutre
24 (2006) show that during boreal winters the albedo of snow in the presence of grass is about
25 0.8 (contributing to the cooling of the atmosphere). The presence of trees, however, reduces
26 the albedo to 0.4 and consequently increases the temperature in the atmosphere. Denman et
27 al. (2007) also show that “Shorter vegetation with more leaves has the most latent heat flux
28 and the least sensible flux. Replacement of forests with shorter vegetation together with the
29 normally assumed higher albedo could then cool the surface”. Vegetation induced
30 cooling/warming through albedo change is also discussed in several other studies

1 (Ganopolski et al., 1998; Claussen, 1998; Claussen et al., 2006; Kubatzki et al., 2000).

3 3.1. JJA surface temperature anomalies

4
5 CCSM3 and LOVECLIM simulate a significant warming over almost all the continents in JJA
6 during MIS-5e, with the largest warming over the NH lands (Figure 2). The large continental
7 warming during MIS-5e results from its much higher insolation during boreal summer.
8 Radiative forcing induces a temperature response larger over land than over the ocean due to
9 the large thermal capacity of the ocean. Differences in heat capacity can explain the large
10 variation between land and ocean surface during boreal summer are warmer. Significant
11 warming is simulated over North America, Asia and Europe, in line with reconstructed surface
12 temperatures (Beaulieu and Reille, 1992; Hahne et al., 1994; Laberyie et al., 1995;
13 Mamakowa, 1989). Table 3 gives some reconstructed surface temperature anomalies at
14 different locations as well as the corresponding results in both models. The significant
15 warming over Asia is in line with the loess records in China which indicate warm and humid
16 conditions during the last interglacial (Porter, S., 2001; Guan et al., 2007). Over China, both
17 CCSM3 and LOVECLIM simulate cooler annual temperature during MIS-5e, but warmer
18 summer, confirming that the strength of the soil development in the loess reflects mostly the
19 summer climatic conditions. Cooling is simulated over the monsoon region of North Africa,
20 related to a strengthened African monsoon (see section 4). The cooling is mainly driven by
21 increased low level moisture and latent heat flux in both models, increased cloudiness and
22 precipitation in CCMS3 and increase in precipitation and vegetation feedback in LOVECLIM.
23 Fischer and Jungclaus (2010) also simulated a temperature decrease in the tropics attributed
24 to the same intensification of the African monsoon system. Intensive warming is simulated in
25 the Arctic (for 60°N to 90°N) in both models. The simulated warming in CCSM3 is 2.2°C and
26 in LOVECLIM is 3°C, in agreement with the warming of 2.4°C found by means of numerical
27 simulations in Otto-Bliesner et al. (2006a). This warming is caused by the high insolation at
28 the top of the atmosphere during JJA and the large reduction of the sea ice and snow cover.
29 Less sea ice is simulated in both models - about -40% in CCSM3 and up to -60% in
30 LOVECLIM (Figure 3). The sea-ice models of CCSM3 and LOVECLIM are both dynamic and

1 thermodynamic, but it is only one sea-ice thickness category in LOVECLIM but multi-category
2 in CCSM3. This difference in sea-ice category at least partly contributes to the different sea-
3 ice response in the two models. Additionally, the reduction of snow cover (not shown) in
4 Greenland and on the islands west of Greenland, is simulated to be up to 8m in LOVECLIM
5 and up to 1m in CCSM3. The strong feedback from the reduction of snow cover over land,
6 next to the external astronomical forcing, could partly explain why Greenland is on average
7 warmer in LOVECLIM (5.3°C) than in CCSM3 (3.4°C). The simulated warming for 75.10°N
8 and 42.32°W in CCSM3 is 3.8°C and in LOVECLIM is 6.3°C in line with the warming of about
9 5°C found in ice-core record (Andersen et al., 2004). Duplessy et al. (2007) point out that the
10 summer temperatures were 2° to 5°C warmer than today in North Atlantic, Greenland
11 (Andersen et al., 2004), Alaska (Muhs et al., 2001) and Asia (Lozhkin and Anderson, 1995)
12 (Table 3). Anderson et al. (2006) reviewed the Arctic climate during the last interglacial based
13 on reconstructed proxy records in terrestrial and marine archives. These reconstructions
14 show that the Arctic summer temperatures were about 4-5°C warmer than today and
15 associated with a decrease in summer sea ice.

16
17 Over Antarctica the simulated mean surface temperature anomaly between 70°S and 90°S is
18 0.4°C in CCSM3 and 3.1°C in LOVECLIM. This warming is driven by the global warmth during
19 MIS-5e and the extent of sea ice (Figure 3). Warming is found between both model
20 simulations near the shelves of Antarctica in the regions of decreased sea-ice concentration.
21 The decrease of the sea-ice concentration causes a release of heat from the ocean into the
22 atmosphere due to its lowered insulation. CCSM3 simulates more sea ice, extending further
23 to the North during MIS-5e than does LOVECLIM. This is related to the enhanced meridional
24 temperature gradient between Africa and the Southern Ocean and increased upper level
25 zonal wind (Otto-Bliesner et al., 2006b; Yeager et al., 2006; Gent et al., 2011; Herold et
26 al., 2012). In west Antarctic Peninsula, LOVECLIM underestimates the sea-ice extent (Goosse
27 et al., 2010), leading to larger positive temperature differences with PI than in CCSM3. Over
28 the Southern Ocean LOVECLIM SST anomaly remains higher than the anomaly in CCSM3
29 but both being lower than the findings in proxy records. Marine records show a warming of
30 about 2°C over the Southern Ocean during the last interglacial period (Labeyrie et al., 1999;

1 Pahnke et al., 2003).

2

3 **3.2. DJF surface temperature anomalies**

4

5 During boreal winter both models show cooler continents in MIS-5e than at PI (Figure 4), as a
6 consequence of its reduced insolation. East of Japan, a negative anomaly is simulated in
7 CCSM3 associated with an increased sea-ice formation, but not in LOVECLIM (Figure 5).
8 Over the oceans, the sea-surface temperature (SST) anomalies are weak in both models
9 (around -0.5°C). In the southern polar region (for 60-90°S), CCSM3 and LOVECLIM simulate
10 an average cooling of -1.8° and -0.3°C, respectively. However, over the Southern Ocean, both
11 models simulate areas of warming. Between 52°S and 59°S and 40°E and 35°W CCSM3 and
12 LOVECLIM simulate a warming of 0.2° and 0.6°C, respectively (see Table 3). Nonetheless,
13 both models underestimate the warming of 2-3.5°C given in the proxy record by Bianchi and
14 Gersonde (2002). Similarly, around 55°S at 160°E, CCSM3 and LOVECLIM underestimate
15 the warming of 5-6°C found in Crosta et al. (2004).

16

17 Over most of the Arctic region, the surface temperature anomalies agree pretty well in both
18 models with a smooth south-north transition from cooling to warming. The winter Arctic SST in
19 MIS-5e remains higher than in PI, a result of the higher summer insolation and its delayed
20 impact in winter through the ocean-sea-ice system, the so-called summer remnant effect (Yin
21 and Berger, 2012). Fischer and Jungclaus (2010) also point out that the reduced/absent sea-
22 ice cover over the Barents Shelf and on the east coast of Greenland cannot act as an
23 insulator between the ocean and the atmosphere and heat from the ocean is released in DJF.
24 The Arctic, for 60-90°N, remains warmer in LOVECLIM partly related to the snow cover
25 change, too. In LOVECLIM the anomaly is -0.5m and in CCSM3 it is -0.01m. This is mainly
26 attributed to the melting of snow over Greenland where the role of snow depth is important
27 due to its effect on albedo. A vegetation feedback could also be related to the simulated
28 warmth in LOVECLIM. LOVECLIM surface temperature in MIS-5e remains higher than in
29 CCSM3 in the areas of expanded vegetation during MIS-5e. However, CCSM3 do not
30 account for the MIS-5e vegetation, hence it will be difficult to assess its effect on surface

1 temperature. Discrepancy on the sign of the anomalies between the two models happens in
2 the area of Svalbard archipelago from 74° to 81°N and from 10° to 35°E. CCSM3 simulates a
3 large cooling of -4.5°C while LOVECLIM simulates a warming of 6.4°C, mirrored also in the
4 sea-ice concentration in Figure 5. CCSM3 shows a sea-ice expansion with its maximum
5 positive anomaly (more than 20%) during DJF. Herold et al. (2012) first point the appearance
6 of such intensified sea-ice expansion after a 800 years run. Possible reason for this sea-ice
7 expansion could be related to the freshening and cooling of the North Atlantic Current. This
8 would induce two effects: a sea-ice increase at around 45°N and 60°W and a transport of
9 fresh and cold waters to the Greenland and Norwegian seas resulting in an increased sea-ice
10 formation. The decrease in salinity (not shown) in CCSM3 and LOVECLIM as a result of sea-
11 ice melting during boreal summer indicates a freshening that is consistent with the weakening
12 of the Atlantic Meridional Overturning Circulation (AMOC) simulated in both models during
13 MIS-5e relative to PI. For example, in LOVECLIM, the much higher NH summer insolation
14 during MIS-5e reduces significantly the NH sea-ice concentration and increases the
15 temperature of the source region of North Atlantic deep water all year round, leading to a
16 weaker North Atlantic deep water formation during MIS-5e than PI (Yin, 2013). Oppo et al.
17 (2001) discuss that changes in latitudinal temperature gradients may induce changes in large-
18 scale wind fields with “far-reaching influences”. Such influences include, for example,
19 changes in the strength and/or position of the Atlantic Meridional Overturning Circulation
20 (Hodell et al., 2009), changes in temperature and salinity in areas of deep water formation,
21 etc. Bauch et al. (1999) investigated the sea-surface temperature in the area of Iceland,
22 Norwegian and Greenland Seas based on proxy records of planktonic foraminiferal
23 assemblages, CaCO₃ content, oxygen isotopes of foraminifera and iceberg-rafted debris.
24 Based on this analysis, it was shown that MIS-5e SST was warmer in comparison with
25 Holocene in Iceland Sea, but remained cooler north of 70°N due to a reduction in the
26 northward flow of Atlantic surface water, less outflow of polar waters from the Arctic Ocean
27 and steeper meridional SST gradient. It was also suggested that a relatively cold northern
28 Eurasian margin could have resulted in more glaciated areas with consequences for the
29 atmospheric circulation patterns, sea-ice cover and albedo.

30

1 **3.3 Annual surface temperature anomalies**

2

3 Figure 6 shows the annual differences between MIS-5e and PI simulated by CCSM3 and
4 LOVECLIM. Warming is simulated in high latitudes by both models with the largest anomalies
5 towards the North Pole. This warming is a result of the high insolation during summer and the
6 summer remnant effect during winter (Yin and Berger, 2012). On the contrary, over the
7 Southern Ocean, the insolation change during DJF is too small to trigger a summer remnant
8 effect and the annual warming is driven by the global warmth during JJA. Warmer Southern
9 Ocean and an annually warmer Antarctica are modeled in LOVECLIM, but not in CCSM3. The
10 average anomaly for the area 70-90°S is 1.5°C in LOVECLIM and -0.2°C in CCSM3 (see
11 Table 3). The warming in LOVECLIM is in line with ice-core records from the Antarctic
12 Plateau. The Vostok ice core shows an average warming of 2.3°C (Petit et al., 1999), which
13 was confirmed later by the EPICA ice-core record showing a 2-4°C warming during MIS-5e
14 compared to PI (Jouzel et al., 2007; Masson-Delmotte et al., 2010).

15 Overall, the annual mean response of the two models is small, but the seasonal response is
16 much clearer. This is also discussed by Lunt et al. (same issue) in their model
17 intercomparison. They stress that the agreement between models and proxy records is far
18 from perfect and it is important to assess the uncertainties in these proxy records. LOVECLIM
19 simulates higher seasonal and therefore annual mean surface temperatures than CCSM3.
20 Around Svalbard archipelago the strong DJF signal, simulated in CCSM3, is imprinted on the
21 annual surface temperature whereas the JJA signal dominates the LOVECLIM simulations in
22 this region. The uncertainties remain large in the areas of modeled sea-ice formation and
23 need to be further addressed because the majority of the seasonal and annual temperature
24 variations occur at the sea-ice boundaries.

25

26 **4. Simulated precipitation anomalies**

27

28 **4.1. JJA precipitation anomalies**

29

30 Monsoon is the major manifestation of the seasonal cycle in the tropical regions and there is a

1 wide range of evidence from marine and terrestrial data that the monsoon characteristics are
2 affected by changes in the Earth's astronomical parameters (Noblet et al., 1996; Kubatzki et
3 al., 2000; Montoya et al., 2000) during the last Interglacial. Both CCSM3 and LOVECLIM
4 simulate significantly stronger northern monsoon during MIS-5e. Compared to PI (Figure 7),
5 the rainfall increases by 4-5 mm/day during MIS-5e over central Africa and Saudi Arabia and
6 by 3-4 mm/day over India, Tibet, southwestern China and the northern part of South America.
7 These results are in good agreement with the simulated heavy precipitation and proxy-based
8 reconstruction reported in Prell and Kutzbach (1987). The precipitation change is relatively
9 small over the extra-tropical regions.

10 A strong northward migration of the Intertropical Convergence Zone (ITCZ) was simulated in
11 equatorial Africa with a significant precipitation increase over the Sahel and southern Sahara,
12 but less over tropical Africa south of 8°N. The sources of water for our simulated African
13 monsoon are from the tropical Atlantic and from local recycling further inland. The amount of
14 water vapor coming from both sources is enhanced during the last Interglacial due to
15 increased low-level wind speeds and land evaporation rates, as discussed also in Braconnot
16 et al. (2008). Indeed the distribution of precipitation depends very much on the location of
17 moisture sources and on wind speed. Compared to PI, the increased low level wind speed
18 and moisture transport during MIS-5e are consistent in both model simulations showing
19 higher tropical boreal summer precipitation.

20 Over Asia the most prominent shifts in precipitation maxima is related to the northward
21 displacement of the ITCZ. Northward shift of the ITCZ during JJA is seen from the eastern
22 Pacific to India, consistent with a greater increase in JJA insolation in the NH compared to the
23 SH. The warmer summer and colder winter lead to larger NH seasonal contrast. Large
24 amounts of water vapor are advected from moisture sources located over the Arabian Sea,
25 the Indian Ocean and west Pacific to Southern Asia. Moreover the northward penetration of
26 moist air is limited by the Tibetan plateau that prevents it from being transported further north.
27 As a consequence Asia experienced stronger summer monsoon in MIS-5e. The southern and
28 western branch of the North Pacific high strengthens the East Asian summer monsoon as
29 seen from an increase in onshore winds and in precipitation in northern China for CCSM3 and

1 in most of China in LOVECLIM. Southwesterly surface wind over India, cross equatorial flow
2 over Indian Ocean and anticyclonic circulation over western North Pacific Ocean are stronger
3 in CCSM3 than in LOVECLIM (Figure 8). The surface wind and moisture transport (not
4 shown) during MIS-5e are in good agreement with water vapor supply over East Asia coming
5 mainly from Indian Ocean and secondarily from South China Sea and western Pacific Ocean.

6
7 Monsoon rainfall distribution is closely related to large scale atmospheric circulation. The
8 simulated upper level (200 hPa) tropical easterly jet (TEJ) anomaly is stronger in CCSM3 than
9 LOVECLIM over a region of 5-20°N and 150-210°E (Figure 9). The mean change over this
10 region is 1.06 m/s for CCSM3 and -0.91 m/s for LOVECLIM. TEJ is closely linked to the
11 boreal summer monsoon rainfall over Africa and Asia through the Hadley circulation. We
12 found that TEJ was stronger and shifted northward from its mean position during MIS-5e,
13 consistent with the strong rainfall over the convergence zone between the wind of the
14 southern and northern hemispheres, known as the monsoon trough (Zeng and Guo, 1982).
15 Similarly, Bosman et al. (2012) found a weakened African Easterly jet but strengthened TEJ
16 with north and westward extensions. Therefore, strong TEJ could be a dominating factor for
17 stronger monsoon over Indian and African region. Another important component of the
18 summer monsoon circulation is the upper-level monsoon ridge (in the 200 hPa geopotential
19 height), which normally extends from the Middle East eastward to southeastern Asia. The
20 northward shift of the strong gradient indicates a strong divergence in the upper troposphere
21 which supports the strong monsoon meridional vertical circulation and heavy rainfall over that
22 region. An anomalous high over central Europe, a low over the western Siberia plain and a
23 major high anomaly over northeastern Asia depict a wave train that has an equivalent
24 barotropic structure in the mid-latitudes. The specific humidity anomaly seen at low level
25 favours also the heavy rain simulated over Africa, India and East Asia. The JJA vertical
26 velocity at 400 hPa between 0-40 °N indicates more convection and heavier rainfall especially
27 over the African and Asian domains (Figure 10). The Indian Monsoon Index (IMI) is defined by
28 the difference between the 850 hPa zonal wind averaged over the region of 5-15°N and 40-
29 80°E and that averaged over the region of 20-30°N and 70-90°E (Wang and Fan, 1999). The
30 Indian summer monsoon component plays dominant role in over all performance of Asian

1 summer monsoon. The simulated JJA IMI is definitely stronger, by 0.13 in the 100-year mean
2 in CCSM3, during MIS-5e (Figure 11) than PI. This change is statistically significant and well
3 represents the change in precipitation over the Indian region.

4

5 There is more monsoon precipitation in the NH during MIS-5e in LOVECLIM than in CCSM3
6 (Table 4). A major precipitation difference between two models is found over tropical Indian
7 Ocean, tropical central Pacific Ocean, tropical Atlantic Ocean, North America and East Asia.
8 For example over East Asia, in LOVECLIM, summer precipitation increases over southern
9 and eastern China and over Japan during MIS-5e when compared to PI. This is in agreement
10 with some proxy records. For example, stalagmite from eastern China (Wang et al., 2008) and
11 lake sediments from Japan (Xiao et al., 1999) indicate stronger summer monsoon
12 precipitation during MIS-5e than today. However, CCSM3 simulates less summer precipitation
13 over eastern China and Japan during MIS-5e than PI.

14

15 **4.2. DJF precipitation anomalies**

16

17 In DJF, both CCSM3 and LOVECLIM simulate more rain during MIS-5e over the Indian
18 Ocean, west Pacific, north east and south east Pacific, but less over the subtropical southern
19 continents (South America, central Africa, and Australia) (Figure 12). The weakening of the
20 southern summer monsoon during MIS-5e is in agreement with the modeling results of
21 Montoya et al. (2000) and with some proxy records. For example, Tofalo et al. (2011)
22 conclude a drier MIS-5e in Argentina based on their analysis of loess-paleosols records. High
23 pollen concentrations and high percentage of henopodiaceae/Amaranthaceae from the lake
24 Titicaca (Bolivia-Peru) indicate warmth and aridity during MIS-5e (Fritz et al., 2007). Zhao et
25 al. (2001) shows that the stalagmite growth in Western Australia during MIS-5e was slow
26 implying dry conditions. Ayliffe et al. (1998) discuss that during interglacials and warm
27 interstadials the southeastern part of Australia was comparatively arid. Therefore, both model
28 simulations and proxy data show a weakened monsoon precipitation in the SH during MIS-5e
29 compared to PI.

1

2 **5. Vegetation**

3

4 Over Africa (between the Equator and 30°N), the increase of tree fraction during MIS-5e as
5 compared to PI is larger in LOVECLIM than in BIOME4 (Figure 13a, d). Grassland simulated
6 in BIOME4 (Figure 13b) occupies about 80% of the land at 20°N while LOVECLIM simulates
7 about 50%, the rest being mainly trees (Figure 13e). On one hand, this difference between
8 the two models could be related to the fact that the vegetation-climate feedbacks are missing
9 in CCSM3 due to the lack of a dynamic vegetation model. On the other hand, it could be
10 related to the fact that LOVECLIM tends to overestimate the precipitation around 30°N and
11 the temperature in the tropics (Goosse et al., 2010) and therefore to amplify the vegetation
12 response. This has also been reflected in the inter-model comparison for the mid-Holocene
13 climate (Braconnot et al. 2007). The expansion of the vegetated area during MIS-5e in
14 Sahel/Sahara in LOVECLIM, which results from the northward shift of the ITCZ and moisture
15 advection, is in line with proxy records showing wetter, more green and vegetated
16 Sahel/Sahara (Jolly et al., 1998).

17

18 Simulated grass is also more developed over Europe, Asia and central North America
19 (between 30°N and 60°N) in BIOME4 during MIS-5e than in LOVECLIM. The abundance of
20 grass and decrease of forest in BIOME4 could be associated with colder annual climate and
21 negative precipitation anomaly in CCSM3 that could affect the distribution of vegetation.
22 LOVECLIM simulates warmer annual climate and positive precipitation anomaly with higher
23 tree fraction below 45°N and similar between 45°N and 60°N to its PI level, in line with proxy
24 data showing a well-established mixed forest in Europe (Kukla et al., 2002; Muller et al., 2003;
25 Shackleton et al., 2003). The simulation of BIOME4 over the Chinese loess plateau shows
26 temperate deciduous forest, temperate conifer forest and warm mixed forest in the south and
27 central part of the loess plateau, and cool mixed forest, shrubland and grassland in the
28 northwestern part. The simulation of LOVECLIM shows that trees are mainly developed in the
29 south region (>50%) while grass occupies more space in the northwestern part. Both model
30 simulations are found in agreement with proxy data over the Chinese loess plateau showing a

1 mixture of steppe and forest (Cai et al., 2012).
2 To the north (between 60°N and 70°N), wetter and warmer climate promote the growth and
3 northward shift of boreal forest in both models (Figure 13a, d). Based on fossil pollen data,
4 Anderson et al (2006) report that the boreal forests experienced “dramatic poleward
5 expansions”. Tundra, grass and forest (proxy data indicate mainly birch forest) flourished on
6 the western and eastern sides of Greenland. Notable northward shift of boreal forest across
7 the Arctic is also reported in Saarnisto et al. (1999) for Scandinavia, in Lozhkin et al. (2007)
8 for Siberia and in Edwards et al. (2003) for Alaska.

9
10 A large reduction in deserts, as compared to PI, is simulated by both BIOME4 and LOVECLIM
11 over the NH (Figure 13c, f). Over the Southern Hemisphere, good agreement is also found
12 between the two models. The increase in desert between the Equator and 30°S is attributed
13 to the annual warming and decreased precipitation over Australia.

14 15 **6. Mean climate and interannual variability of the tropical Pacific**

16
17 To study the changes in the mean climate of the tropical Pacific, the annual mean of
18 equatorial tropical Pacific SST, zonal wind stress and mean tilt of the thermocline are
19 averaged over 5°S-5°N between 150-275°E and analyzed. In the CCSM3 simulations, MIS-5e
20 SST shows a westward shift in the Pacific cold tongue (minimum SST), an eastward shift of
21 the warm pool (maximum SST) and a cooling mainly in the central Pacific relative to the PI
22 (Figure 14a). The east-west SST difference (difference between cold tongue and warm pool)
23 increases slightly from 4°C in PI to 4.2°C in MIS5. This is not the case for LOVECLIM which
24 shows, in both MIS-5e and PI, an east-west SST difference of 2°C. For CCSM3, the zonal
25 wind stress shows a very slight decrease mainly in the eastern and western sides in MIS-5e
26 (Figure 14b). In LOVECLIM, however, there is a significant increase in the MIS-5e zonal wind
27 stress when compared to PI. The mean thermocline depth (depth of the largest vertical
28 temperature gradient) is approximated by the depth of the 20°C-isotherm as is usually done
29 by model studies of PI and also found to be a good approximation for MIS-5e. In CCSM3,
30 there is almost no difference in the thermocline between MIS-5e and PI (Figure 14c) which is

1 consistent with the very small difference in the zonal wind stress. In contrast, LOVECLIM
2 shows a much deeper thermocline for MIS-5e especially in the western part. Based on the
3 finding of Timmermann et al. (2005), we suggest that this deepening of the thermocline is an
4 ocean-related process most likely caused by its re-adjustment to the weakening of the Atlantic
5 meridional circulation (AMOC) as mentioned earlier. The thermocline deepening occurring
6 only in LOVECLIM but not in CCSM3 might be related to the difference in their atmosphere
7 resolutions. Indeed, in response to AMOC weakening, more complex models exhibit a change
8 in their atmospheric circulation which in turn causes a shoaling of the thermocline and
9 restrains the thermocline from deepening through oceanic processes (Timmermann et al.,
10 2007a).

11 For the interannual variability around the mean state discussed above, the last 1200 months
12 of SSTs were analyzed. We focus on the so-called NINO3.4 region (5°S-5°N; 190 -240°E) and
13 the SST averaged over this region. The monthly mean cycle was resolved, and a 12-month
14 moving average filter was applied following Douglass (2011). The NINO3.4 SST variability in
15 the LOVECLIM simulations is particularly small (Figure 15b). This is because the
16 overestimated deep thermocline in LOVECLIM diminishes the SST variability. Underestimated
17 SST variability in LOVECLIM was also mentioned by Goosse et al. (2010). We will, therefore,
18 mainly discuss the ENSO characteristics of the CCSM3 experiments.

19 The spectrum of the SST NINO3.4 anomalies shows dominant variability at interannual time
20 scale which is related to ENSO (Figure 15a). The spectrum power for PI has large and
21 significant magnitude in 1.7-6.5 year band with the largest peak around 3.7 years. We also
22 find the largest peak of the spectrum at period around 2-3 years when we apply a 5-month
23 moving average filter. This is consistent with some other CCSM3 model studies where a
24 period of around 2 years for ENSO variability was found (e.g., Merkel et al., 2010). In the MIS-
25 5e run, the large and significant peaks of the spectrum are limited to 2-6 year band while the
26 leading period is around 2.1 years. The largest peak of the power spectrum in MIS-5e has
27 shorter period compared to the one in PI and its magnitude is slightly larger (~10%). This
28 shorter period during MIS-5e might be partially related to the westward shift of the cold tongue
29 which reduces the distance between the cold tongue and the warm pool. The moderate
30 change in the magnitude and pattern of the significant peaks in the spectrum of MIS-5e can in

1 some degree be related to the shoaling of the thermocline, the increase of the east-west
2 temperature gradient and the weaker trade winds in the tropical Pacific. However, as shown
3 above, the change in these factors was moderate. It is also of interest to check other factors.
4 Following Timmermann et al. (2007b), the change in the strength and phase of the SST
5 annual cycle (mean value of each month) could be another factor to modify the power
6 spectrum in MIS-5e. This can be further investigated by comparing the annual cycle with
7 standard deviation of each month as inspired by Merkel et al. (2010). The standard deviation
8 (Figure 15b) and the mean SST (Figure 15c) of each month do not follow the same trend
9 (have opposite trend). The standard deviation of the MIS-5e SST is the highest (lowest) in
10 boreal winter (spring) when the amplitude of the annual cycle is around its minimum
11 (maximum) which might affect the ENSO variability. Measurement of oxygen isotopes in coral
12 fossils of Bunaken Island (around 120°E of the equator) by Hughen et al. (1999) also showed
13 ENSO variability but suggested the same power spectrum as the SST data prior to 1976.

14

15 **7. Conclusions**

16

17 In this paper, the last interglacial climate, including surface temperature, hydrological cycle,
18 vegetation and ENSO, was investigated through simulations of two models of different
19 complexity, CCSM3 and LOVECLIM. In both models, continents remain warmer during
20 summer (except over North Africa and Arabian Peninsula) and cooler during winter in MIS-5e
21 than PI. Discrepancies between the two models mainly occur in the polar areas, closely
22 related to feedbacks from sea ice and snow cover. CCSM3 simulates more sea ice in MIS-5e
23 and lower surface temperatures than LOVECLIM. In addition, the reduction in snow is much
24 larger cover in LOVECLIM than in CCSM3, contributing to the larger Arctic warming in
25 LOVECLIM.

26 Intensification of the African monsoon causes cooling during boreal summer over North Africa
27 and on the Arabian Peninsula. In MIS-5e the ITCZ moves further north as compared to PI.
28 Precipitation increases over the Sahel/Sahara, over India, Tibet, southwestern China and over
29 the northern part of South America. Deserts reduce largely in the NH, but increase in North
30 Australia due to the annual warming and decreased precipitation. Trees and grassland

1 flourish in Sahel/Sahara, trees being more abundant in LOVECLIM simulation than in
2 BIOME4. Simulated mid-latitude trees are also more abundant in LOVECLIM. In both models
3 trees expand deep in high northern latitudes, found in good agreement with proxy records..
4 CCSM3 simulates larger tropical Pacific SST for MIS-5e than for PI. We suggest this is
5 related to the change in the SST annual cycle next to smaller effects through increased east-
6 west temperature gradient and less-steep thermocline. The SST variability in our LOVECLIM
7 simulations is particularly small due to the overestimated thermocline's depth.

8

9 The simulated broad-scale climate change during the last interglacial as compared to PI is
10 compared well between the two models. This demonstrates that LOVECLIM, although
11 classified as a climate model of intermediate complexity, is an efficient tool for climate
12 investigations. Additionally, CCSM3 and LOVECLIM qualitatively simulate the large scale
13 climate changes in line with proxy records. We should keep in mind that the proxy records are
14 scarce and mostly confined to the NH and their interpretations are regionally biased.
15 Additional proxy data could increase not only our understanding of the past climate dynamics,
16 but can provide necessary data for model assessment because comparisons between model
17 simulations and proxy data is a key to test the credibility of the proposed methods.

18

19 **Acknowledgments**

20

21 This work and I. Nikolova, U. K. Singh and M. P. Karami are supported by the European
22 Research Council Advanced Grant EMIS (No 227348 of the Program 'Ideas'). Q. Z. Yin is
23 supported by the Belgian National Fund for Scientific Research (F. R. S. -FNRS). N. Herold is
24 thanked for the simulations with CCSM3. Access to computer facilities was made easier
25 through sponsorship from S. A. Electrabel, Belgium. Computational resources have been
26 provided by the supercomputing facilities of the Université Catholique de Louvain (CISM/UCL)
27 and the Consortium des Equipements de Calcul Intensif en Fédération Wallonie Bruxelles
28 (CECI) funded by the Belgian National Fund for Scientific Research (FRS-FNRS).

29

30 **References**

- 1
- 2 An, Z. S., Liu, T. S., Lu, Y. C., Porter, S. C., Kukla, G., Wu, X. H. and Hua, Y.: The long-term
3 paleomonsoon variation recorded by the loess-paleosol sequence in central China.
4 *Quatern. Int.*, 7, pp. 91–96, 1990.
- 5 Andersen, K.K., Azuma, N., Barnola, J.-M., Bigler, M., Biscaye, P., Caillon, N., Chappellaz, J.,
6 Clausen, H.B., Dahl-Jensen, D., Fischer, H., Flückiger, J., Fritzsche, D., Fujii, Y., Goto-
7 Azuma, K., Grønvold, K., Gundestrup, N.S., Hansson, M., Huber, C., Hvidberg, C.S.,
8 Johnsen, S.J., Jonsell, U., Jouzel, J., Kipfstuhl, S., Landais, A., Leuenberger, M.,
9 Lorrain, R., Masson-Delmotte, V., Miller, H., Motoyama, H., Narita, H., Popp, T.,
10 Rasmussen, S.O., Raynaud, D., Rothlisberger, R., Ruth, U., Samyn, D., Schwander, J.,
11 Shoji, H., Siggard-Andersen, M.-L., Steffensen, J.P.S., T., Sveinbjörnsdóttir, A.E.,
12 Svensson, A., Takata, M., Tison, J.-L., Thorsteinsson, T., Watanabe, O., Wilhelms, F.
13 and White, J.W.C.: High-resolution record of Northern Hemisphere climate extending
14 into the last interglacial period. *Nature*, 431, pp. 147-151, 2004.
- 15 Anderson, P., Bermike, O., Bigelow, N., Brigham-Grette, J., Duvall, M., Edwards, M.E.,
16 Frechette, B., Funder, S., Johnsen, S., Knies, J., Koerner, R., Lozhkin, A.,
17 Marshall, S., Matthiessen, J., Macdonald, G., Miller, G., Montoya, M., Muhs, D., Otto-
18 Bliesner, B., Overpeck, J., Reeh, N., Sejrup, H., Spielhagen, R., Turner, C. and
19 Velichko, A.: Last Interglacial Arctic warmth confirms polar amplification of
20 climate change. *Quaternary Sci. Rev.*, 25, no. 13-14, pp. 1383-1400,
21 doi:10.1016/j.quascirev.2006.01.033, 2006.
- 22 Andreev, A. A., Grosse, G., Schirmer, L., Kuzmina, S. A., Novenko, E. Yu., Bobrov, A. A.,
23 Tarasov, P. E., Ilyashuk, B. P., Kuznetsova, T. V., Krbetschek, M., Meyer, H. and
24 Kunitsky, V. V.: Late Saalian and Eemian paleoenvironmental history of the Bol'shoy
25 Lyakhovsky Island (Laptev Sea region, Arctic Siberia). *Boreas*, 33, pp. 319-348, 2004.
- 26 Ayliffe, L. K., Marianelli, P.C., Moriarty, K. C., Wells, R.T., McCulloch, M. T., Mortimer, G. E.
27 and Hellstrom, J.C.: 500 ka precipitation record from southeastern Australia:
28 evidence for interglacial relative aridity. *Geology*, 26, pp.147-150, 1998.
- 29 Bauch, H. A., Erlenkeuser, H., Fahl, K., Spielhagen, R. F., Weinelt, M. S., Andruleit, H.
30 and Henrich, R.: Evidence for a steeper MIS5 than Holocene sea surface temperature

1 gradient between Arctic and sub-Arctic regions. *Palaeogeogr. Palaeocl.*, 145, pp. 95–
2 117, 1999.

3 Beaulieu, J.-L. de and Reille, M.: The last climatic cycle at La Grande Pile (Vosges, France) -
4 a new pollen profile. *Quaternary Sci. Rev.*, 11, pp. 431-438, 1989.

5 Berger, A.: Long Term Variations of Daily Insolation and Quaternary Climatic Changes.
6 *J. Atmos. Sci.*, 35(12), pp. 2362-2367, 1978.

7 Berger, A. and Loutre, M. -F.: Modélisation de la réponse du climat au forçage astronomique
8 et à la concentration en CO₂. *Comptes rendus de l'Académie des sciences. Série 2.*
9 *Sciences de la terre et des planètes*, 323 (1), pp. 1-16, 1996.

10 Berger, A. and Yin, Q. Z.: Modelling the past and future interglacials in
11 response to astronomical and greenhouse gas forcing, *The Future of the World's*
12 *Climate*, Elsevier, Amsterdam. ISBN: 9780123869173. pp. 437–462, 2012.

13 Bianchi, S. and Gersonde, R.: The Southern Ocean surface between Marine Isotope Stages
14 6 and 5d: shape and timing of climate changes. *Palaeogeogr. Palaeocl.*,
15 187, Issue 1-2, pp. 151-177, 2002.

16 Bintanja, R., Wal, van de and Oerlemans, J.: Modelled atmospheric temperatures and global
17 sea levels over the past million years. *Nature*, 437, pp. 125-128, 2005.

18 Bosman, J. H. C., Drijfhout, S. S., Tuenter, E., Lourens, L. J., Hilgen, F. J and Weber, S. L.:
19 Monsoonal response to mid-holocene orbital forcing in a high resolution GCM. *Clim.*
20 *past*, 8, pp. 723-740, 2012.

21 Braconnot, P., Harrison, S. P., Joussaume, S., Hewitt, C. D., Kitoch, A., Kutzbach, J. E.,
22 Liu, Z., Otto-Bliesner, B., Syktus, J. and Weber, S. L.: Evaluation of PMIP coupled
23 ocean-atmosphere simulations of the mid-Holocene. *Dev. Paleoenviron. Res.*, 6,
24 pp. 515-533, 2004.

25 Braconnot, P., Otto-Bliesner, B., Harrison, S., Joussaume, S., Peterchmitt, J.-Y., Abe-Ouchi,
26 A., Crucifix, M., Driesschaert, E., Fichefet, Th., Hewitt, C. D., Kageyama, M., Kitoch,
27 A., Laine, A., Loutre, M.-F., Marti, O., Merkel, U., Ramstein, G., Valdes, P.,
28 Weber, S. L., Yu, Y. and Zhao, Y. : Results of PMIP2 coupled simulations of the
29 Mid-Holocene and Last Glacial Maximum - Part 1: experiments and large-scale
30 features. *Clim. Past*, 3, pp. 361-277, 2007.

- 1 Braconnot, P., Marzin, C., Gregoire, L., Mosquet, E. and Marti, O.: Monsoon response to
2 changes in Earth's orbital parameters: comparison between simulations of the MIS5
3 and of the Holocene. *Clim. Past*, 4, pp. 281-294, 2008.
- 4 Briegleb, B. P., Bitz, C. M., Hunke, E. C., Lipscomb, W. H., Holland, M. M., Schramm, J. L.
5 and Moritz, R. E.: Scientific description of the sea ice component in the Community
6 Climate System Model, Version Three. Technical Report NCAR/TN-463+STR, National
7 Center for Atmospheric Research, Boulder, CO. 80307-3000, 2004.
- 8 Brovkin, V., Ganopolski, A. and Svirezhev, Y. : A continuous climate-vegetation classification
9 for use in climate-biosphere studies. *Ecol. Model.*, 101, pp. 251-261, 1997.
- 10 Brovkin, V.: Climate-vegetation interaction. *J. Phys IV France*, 12, pp. 57- 52,
11 doi:10.1051/jp4:20020452, 2002.
- 12 Cai, M., Wei, M., Fang, X., Xu, D., Miao, Y. and Wu, F.: Vegetation and climate change during
13 three interglacial periods represented in the Luochuan loess-paleosol section, on the
14 Chinese Loess Plateau. *Quatern. Int.*, in press,
15 <http://dx.doi.org/10.1016/j.quaint.2012.06.041>
- 16 Caillon, N., Severinghaus, J. P., Barnola, J. -M., Chappellaz, J., Jouzel, J. and Parrenin, F.:
17 Estimation of temperature change and of gas age-ice age difference, 108 kyr BP,
18 at Vostok, Antarctica. *J. Geophys. Res.*, 106, pp. 31893–31901, 2001.
- 19 Claussen, Martin: On multiple solutions of the atmosphere-vegetation system in present-day
20 climate. *Glob. Change Biol.*, 4, pp. 549-559, 1998.
- 21 Claussen, M., Fohlmeister, J., Ganopolski, A. and Brovkin, V.: Vegetation dynamics
22 amplifies precessional forcing. *Geophys. Res. Lett.*, 33, L09709,
23 doi:10.1029/2006GL026111, 2006
- 24 Collins, W. D., Rasch, P. J., Boville, B. A., Hack, J. J., McCaa, J. R., Williamson, D. L.,
25 Kiehl, J. T., Briegleb, B., Bitz, C., Lin, S.-J., Zhang, M. and Dai, Y.: Description
26 of the NCAR Community Atmosphere Model (CAM3). Technical Report NCAR/TN-
27 464+STR, National Center for Atmospheric Research, Boulder, Colorado 80307-3000,
28 226 pp, 2004.
- 29 Collins, W., Bitz, C. M., Blackmon, M. L., Bonan, G. B., Bretherton, C. S., Carton, J. A.,
30 Chang, P., Doney, S. C., Hack, J. J., Henderson, T. B., Kiehl, J. T., Large, W. G.,

1 McKenna, D. S., Santer, B. D. and Smith, R. D.: The Community Climate
2 System Model Version 3 (CCSM3). *J. Climate*, 19, pp. 2122-2143, 2006.

3 Crosta, X., Sturm, A., Armand, L. and Pichon, J.-J.: Late Quaternary sea ice history in the
4 Indian sector of the Southern Ocean as recorded by diatom assemblages. *Mar.*
5 *Micropaleontol.*, 50, Issue 3-4, pp. 209-223, 2004.

6 Crucifix, M. and Loutre, M. -F.: Transient simulations over the last interglacial period (126-
7 115 kyr BP): feedback and forcing analysis. *Clim. Dyn.*, 19, pp. 417-433, 2002.

8 Gent, P. R., Danabasoglu, G., Donner, L. J., Holland, M. M., Hunke, E. C., Jayne, S. R.,
9 Lawrence, D. M., Neale, R. B., Rasch, J., Vertenstein, M., Worley, P. H., Yang, Z. L.
10 and Zhang, M.: The community climate system model version 4. *J. Climate*, 24,
11 pp. 4973-4991, 2011.

12 Denman, K.L., Brasseur, G., Chidthaisong, A., Ciais, P., Cox, P. M., Dickinson, R. E.,
13 Hauglustaine, D., Heinze, C., Holland, E., Jacob, D., Lohmann, U., Ramachandran,
14 S., da Silva Dias, P. L., Wofsy, S. C. and Zhang, X.: Couplings Between Changes
15 in the Climate System and Biogeochemistry. In: *Climate Change 2007: The*
16 *Physical Science Basis. Contribution of Working Group I to the Fourth Assessment*
17 *Report of the Intergovernmental Panel on Climate Change* [Solomon, S., Qin, D.,
18 Manning, M., Chen, Z., Marquis, M., Averyt, K.B., Tignor, M. and Miller, H.L. (eds.)].
19 Cambridge University Press, Cambridge, United Kingdom and New York, NY, USA.
20 1009 pages, ISBN 9780521705967, 2007.

21 Ding, Y. and Chan, J.C.L.: The East Asian summer monsoon: an overview. *Meteorol.*
22 *Atmos. Phys.*, 89, pp. 117-142, 2005.

23 Douglas, D. H.: Separation of a signal of interest from a seasonal effect in geophysical data:
24 El Niño/La Niña phenomenon. *International Journal of Geosciences*, 2, pp. 414- 419,
25 doi: 10.4236/ijg.2011.24045, 2011.

26 Duplessy, J. C., Roche, D. M. and Kageyama, M. (2007): The deep ocean during the last
27 interglacial period. *Science*, 316, no. 89, DOI: 10.1126/science.1138582.

28 Edwards, M. E., Hamilton, T. D., Elias, S.A., Bigelow, N.H. and Krumhardt, A.P.: Interglacial
29 extension of the boreal forest limit in the Noatak valley, northwest Alaska:
30 evidence from an exhumed river-cut bluff and debris apron. *Arct. Antarct. Alp. Res.*, 35,

- 1 pp. 460–468, 2004.
- 2 Fischer N. and Jungclaus, J. H.: Effects of orbital forcing on atmosphere and ocean heat
3 transports in Holocene and MIS5 climate simulations with a comprehensive Earth
4 system model. *Clim. Past*, 6, pp. 155-168, 2010.
- 5 Fritz, S. C., Baker, P. A., Seltzer, G. O., Ballantyne, A., Tapia, P., Cheng, H. and Edwards, R.
6 L.: Quaternary glaciation and hydrologic variation in the South American tropics
7 as reconstructed from the Lake Titicaca drilling project. *Quaternary Res.*, 68 (3), pp.
8 410-420, 2007.
- 9 Ganopolski, A., Kubatzki, C., Claussen, M., Brovkin, V. and Petoukhov, V.: The influence of
10 vegetation-atmosphere-ocean interaction on climate during the Mid-Holocene. *Science*,
11 280, pp. 1916-1919, 1998.
- 12 Goosse, H. and Fichefet, T.: Importance of ice-ocean interactions for the global ocean
13 circulation: a model study, *J. Geophys. Res.*, 104 (C10), pp. 23337–23355, 1999.
- 14 Goosse, H., Brovkin, V., Fichefet, T., Haarsma, R., Huybrechts, P., Jongma, J., Mouchet, A.,
15 Selten, F., Barriat, P. -Y., Campin, J. -M., Deleersnijder, E., Driesschaert, E., Goelzer,
16 H., Janssens, I., Loutre, M. -F., Morales Maqueda, M. A., Opsteegh, T., Mathieu, P. -P.,
17 Munhoven, G., Pettersson, E. J., Renssen, H., Roche, D. M., Schaeffer, M. Tartinville,
18 B., Timmermann, A. and Weber, S. L.: Description of the Earth system model of
19 intermediate complexity LOVECLIM version 1.2. *Geoscience Model Development*, 3,
20 pp. 603-633, 2010.
- 21 Groll, N., Widmann, M., Jones, J. M., Kaspar, F. and Lorenz, S. J.: Simulated relationships
22 between regional temperatures and large-scale circulation: 125 kyr BP (MIS5) and the
23 preindustrial period. *J. Climate*, 18, pp. 4032-4055, 2005.
- 24 Guan, QY., Pan, BT., Gao, HS., Li, BY., Wang JP. And Su, H.: Instability characteristics
25 of the East Asian Monsoon recorded by high resolution loess sections from the last
26 interglacial (MIS5). *Sci. China Ser. D*, 50, pp. 1067-1075, 2007.
- 27 Hahne, J., Kemle, S., Merkt, J. and Meyer, K.-D.: Eem-,weichsel- und saalezeitliche
28 Ablagerungen der Bohrung "Quakenbrück GE 2". *Geologisches Jahrbuch A*, 134, pp.
29 9-69, 1994.
- 30 Harrison, S. P. and Prentice, C.I.: Climate and CO2 controls on global vegetation

1 distribution at the last glacial maximum: Analysis based on palaeovegetation data,
2 biome modelling and palaeoclimate simulations. *Glob. Change Biol.*, 9,
3 pp. 983-1004, 2003.

4 Herold, N., Yin, Q. Z., Karami, M. P. and Berger, A.: Modelling the climatic diversity of the
5 warm interglacials. *Quaternary Sci. Rev.*, 56, pp. 126-141, 2012.

6 Hodell, D. A., Minth, E. K., Curtis, J. H., McCave, I. N., Hall, I. R., Channell, J. E. T. and Xuan,
7 C.: Surface and deep-water hydrography on Gardar Drift (Iceland Basin) during
8 the last interglacial period. *Earth Planet. Sc. Lett.*, 288, pp. 10-19, 2009.

9 Holden, P. B., Edwards, N. R., Wolff, E. W., Lang, H. J., Singarayer, J. S., Valdes, P. J. and
10 Stocker, T. F.: Interhemispheric coupling, the West Antarctic Ice Sheet and warm
11 Antarctic interglacials, *Clim. Past*, 6, pp. 431-443, 2010.

12 Jolly, D., Prentice, I.C., Bonnefille, R., Ballouche, A., Bengo, M., Brenac, P., Buchet, G.,
13 Burney, D., Cazet, J.-P., Cheddadi, R., Ectorh, T., Elenga, H., Elmoutaki, S., Guiot, J.,
14 Laarif, F., Lamb, H., Lezine, A.-M., Maley, J., Mbenza, M., Peyron, O., Reille, M.,
15 Reynaud-Farrera, I., Riollet, G., Ritchie, J.C., Roche, E., Scott, L., Ssemmanda, I.,
16 Straka, H., Umer, M., Van Campo, E., Vilimumbalo, S., Vincens, A. and
17 Waller, M.: Biome reconstruction from pollen and plant macrofossil data for Africa
18 and the Arabian peninsula at 0 and 6000 years. *J. Biogeogr.*, 25, pp. 1007-1027, 1998.

19 Jouzel, J., Masson-Delmotte, V., Cattani, O., Dreyfus, G., Falourd, S., Hoffmann, G., Minster,
20 B., Nouet, J., Barnola, J. M., Chappellaz, J., Fischer, H., Gallet, J. C., Johnsen, S.,
21 Leuenberger, M., Loulergue, L., Luethi, D., Oerter, H., Parrenin, F., Raisbeck, G.,
22 Raynaud, D., Schilt, A., Schwander, J., Selmo, E., Souchez, R., Spahni, R., Stauffer,
23 B., Steffensen, J. P., Stenni, B., Stocker, T. F., Tison, J. L., Werner, M. and Wolff, E. W.
24 : Orbital and Millennial Antarctic Climate Variability over the Past 800,000 Years.
25 *Science*, Vol. 317, No. 5839, pp.793-797, 2007.

26 Kageyama, M., Peyron, O., Pinot, S., Tarasov, P., Guiot, J., Jousaume, S. and Ramstein, G.:
27 The Last Glacial Maximum climate over Europe and western Siberia: a PMIP
28 comparison between models and data, *Clim. Dynam.*, 17, pp. 23-43, 2007.

29 Kaplan, J. O., Bigelow, N. H., Prentice, I. C., Harrison, S. P., Bartlein, P. J., Christensen, T. R.,
30 Cramer, W., Matveyeva, N. V., McGuire, A. D., Murray, D. F., Razzhivin, V. Y., Smith,

- 1 B., Walker, D. A., Anderson, P. M., Andreev, A. A., Brubaker, L. B., Edwards, M. E., and
2 Lozhkin, A. V.: Climate change and arctic ecosystems II: Modeling,
3 paleodata-model comparisons, and future projections. *J. Geophys. Res.*, 108,
4 doi:10.1029/2002JD002559, 2003.
- 5 Kubatzki, C., Montoya, M., Rahmstorf, S., Ganopolski, A. and Claussen, M.:
6 Comparison of the last interglacial climate simulated by a coupled global model of
7 intermediate complexity and an AOGCM. *Clim. Dynam.*, 16, pp. 799-814, 2000.
- 8 Kukla, G., McManus, J.F., Rousseau, D.D. and Chuine I.: How long and how stable was the
9 last interglacial? *Quaternary Sci. Rev.*, 16 (6), pp. 605–612, 1997.
- 10 Kukla, G. J., Bender, M. L., de Beaulieu, J. L., Bond, G., Broecker, W. S., Cleveringa, P.,
11 Gavin, J. E., Herbert, T. D., Imbrie, J., Jouzel, J., Keigwin, L. D., Knudsen, K. L.,
12 McManus, J. F., Merkt, J., Muhs, D. R., Muller, H., Poore, R. Z., Porter, S. C., Seret, G.,
13 Shackleton, N. J., Turner, C, Tzedakis, P. C. and Winograd, I. J.:
14 Last Interglacial Climates. SGS Staff -- Published Research, Paper 174,
15 <http://digitalcommons.unl.edu/usgsstaffpub/174>, 2002.
- 16 Labeyrie, L., Labracherie, M., Gorfti, N., Pichon, J. J., Vautravers, M., Arnold, M., Duplessy, J.
17 -C., Paterne, M., Michel, E., Duprat, J., Caralp, M. and Turon, J. -L.: Hydrographic
18 changes of the Southern Ocean (southeast Indian sector) over the last 230 kyr.
19 *Paleoceanography*, 11, pp. 57-76, 1996.
- 20 Landais, A., Chappellaz, J., Delmotte, M., Jouzel, J., Blunier, T., Bourg, C., Caillon, N.,
21 Cherrier, S., Malaize, B., Masson-Delmotte, V., Raynaud, D., Schwander, J. and
22 Steffensen, J. P. (2003): A tentative reconstruction of the last interglacial and glacial
23 inception in Greenland based on new gas measurements in the Greenland Ice Core
24 Project (GRIP) ice core. *J. Geophys. Res.*, 108, doi:10.1029/2002JD0003147.
- 25 Lozhkin, A. and Anderson, P.: The last interglaciation in northeast Siberia. *Quaternary Res.*,
26 43, pp. 147-158, 1995.
- 27 Lozhkin, A. V., Anderson, P. M., Matrosova, T. V., and Minyuk, P. S.: The pollen record from
28 El'gygytgyn Lake: implications for vegetation and climate histories of northern
29 Chukotka since the late middle Pleistocene. *J. Paleolimnol.*, 37, pp. 135-153, 2007.
- 30 Lunt, D. J., de Noblet-Ducoudre, N. and Charbit, S.: Effects of a melted greenland ice sheet

1 on climate, vegetation, and the cryosphere. *Clim. Dyn.*, 23, pp. 679–694, 2004.

2 Lunt, D. J., Abe-Ouchi, A., Bakker, P., Berger, A., Braconnot, P., Charbit, S., Fischer, N.,
3 Herold, N., Jungclaus, J. H., Khon, V. C., Krebs-Kanzow, U., Lohmann, G., Otto-
4 Bliesner, B., Park, W., Pfeiffer, M., Prange, M., Rachmayani, R., Renssen, H.,
5 Rossenbloom, N., Schneider, B., Stone, E. J., Takahashi, K., Wei, W. and Yin, Q.: A
6 multi-model assessment of last interglacial temperatures. *Clim. Past Discuss.*, 8, pp.
7 3657-3691, 2012.

8 Mamakowa, K.: Late Middle Polish glaciation, Eemian and Early Vistulian vegetation at
9 Imbramowice near Wrocław and the pollen stratigraphy of this part of the Pleistocene
10 in Poland. *Acta Palaeobotanica*, 29, pp. 11-176, 1989.

11 Masson-Delmotte, V., Stenni, B., Pol, K., Braconnot, P., Cattani, O., Falourd, S., Kageyama,
12 M., Jouzel, J., Landais, A., Minster, B., Barnola, J. M., Chappellaz, J., Krinner, G.,
13 Johnsen, S., Röthlisberger, R., Hansen, J., Mikolajewicz, U. and
14 Otto-Bliesner, B.: EPICA Dome C record of glacial and interglacial intensities.
15 *Quaternary Sci. Rev.*, 29, Issues 1–2, pp. 113–128, 2010.

16 McKay, N. P., Overpeck, J. T. and Otto-Bliesner, B. L.: The role of ocean thermal expansion in
17 last interglacial sea level rise. *Geophys. Res. Lett.*, 38, L14605,
18 doi:10.1029/2011GL048280, 2011.

19 Merkel, U., Prange and M., Schulz, M.: ENSO variability and teleconnections during glacial
20 climates. *Quaternary Sci. Rev.*, 29 (1-2), pp. 86-100, 2010.

21 Montoya, M., von Storch, H. and Crowley, T. J.: Climate simulation for 125 kyr BP with a
22 coupled ocean-atmosphere general circulation model. *J. Climate*, 13, 2000.

23 Muhs, D., Ager, T. A. and Beget, J. E.: Vegetation and paleoclimate of the last interglacial
24 period, central Alaska. *Quaternary Sci. Rev.*, 20, pp. 41-61, 2001.

25 Noblet, N. de, Braconnot, P., Joussaume S. and Masson, V.: Sensitivity of simulated Asian
26 and African summer monsoons to orbitally induced variations in insolation 126, 115
27 and 6 kBP. *Clim. Dynam.*, 12, pp. 589-603, 1996.

28 Oleson, K. W., Dai, Y., Bonan, G. B., Bosilovich, M., Dickinson, R., Dirmeyer, P., Hoffman, F.,
29 Houser, P., Levis, S., Niu, G.-Y., Thornton, P., Vertenstein, M., Yang, Z. -L. and Zeng, X.
30 : Technical description of the Community Land Model (CLM). Technical Report

- 1 NCAR/TN-461+STR, National Center for Atmospheric Research, Boulder, CO. 80307-
2 3000, 174 pp, 2004.
- 3 Oppo, D. W., Keigwin, L. D. & McManus, J.F.: Persistent subtropical climate variability in
4 marine isotope stage 5 and Termination II. *Paleoceanography*, 16 (3), pp. 280-292,
5 2001.
- 6 Opsteegh, J. D., Haarsma, R. J., Selten, F. M. and Kattenberg, A.:
7 ECBILT: A dynamic alternative to mixed boundary conditions in ocean models. *Tellus*,
8 50A, pp. 348–367, 1998.
- 9 Otto-Bliesner, B., Marshall, S.J., Miller, G. H., Hu, A. and CAPE Last Interglacial Project
10 members: Simulating Arctic climate warmth and icefield retreat in the last
11 interglaciation. *Science*, 311, no. 5768, pp. 1751-1753,
12 doi: 10.1126/science.1120808, 2006a.
- 13 Otto-Bliesner, B.L., Tomas, R., Brady, E.C., Ammann, C., Kothavala, Z. and Clauzet, G.
14 : Climate sensitivity of moderate- and low-resolution versions of CCSM3 to
15 preindustrial forcings. *J. Climate*, 19, pp. 2567-2583, 2006b.
- 16 Pahnke, K., Zahn, R., Elderfield, H. and Schulz, M.: 340,000-year centennial scale
17 marine record of Southern Hemisphere climatic oscillation, *Science*, 301, pp. 948–952,
18 2003.
- 19 Petit, J.R. , Jouzel, J., Raynaud, D., Barkov, N. I., Barnola, J. -M., Basile, I., Benders, M.,
20 Chappellaz, J., Davis, M., Delaygue, G., Delmotte, M., Kotlyakov, V. M., Legrand,
21 M., Lipenkov, V. Y., Lorius, C., Pépin, L., Ritz, C., Saltzman, E. and Stievenard,
22 M.: Climate and atmospheric history of the past 420,000 years from
23 Vostok ice core, Antarctica. *Nature*, 399, pp. 429-436, 1999.
- 24 Porter, Stephen C.: Chinese loess record of monsoon climate during the last glacial-
25 interglacial cycle. *Earth-Sci. Rev.*, 54, issue 1-3, pp. 115-128, 2001.
- 26 Prell, W. L. and Kutzbach, J. E.: Monsoon Variability over the Past 150,000 Years.
27 *J. Geophys. Res.*, 92, pp. 8411–8425, 1987.
- 28 Saarnisto, M., Eriksson, B., and Hirvas, H.: Tepsankumpu revisited- pollen evidence of stable
29 MIS5 climates in Finnish Lapland. *Boreas*, 28, pp. 12–22, 1999.
- 30 Shackleton, N. J., Sanchez-Goni, M. F., Pailler, D and Lancelot, Y.: Marine isotope

1 substage 5e and the MIS5 interglacial. *Global Planet. Change*, 36,
2 pp. 151-155, doi:10.1016/S0921-8181(02)00181-9, 2003.

3 Shi, Z., Liu, X. and Cheng, X.: Anti-phased response of northern and southern East Asian
4 summer precipitation to ENSO modulation of orbital forcing. *Quaternary Sci. Rev.*, 40,
5 pp. 30-38, 2012.

6 Smith, R. D. and Gent, P. R.: Reference manual for the Parallel Ocean Program
7 (POP), ocean component of the Community Climate System Model (CCSM2.0 and
8 3.0). Technical Report LA-UR-02-2484, Los Alamos National Laboratory, available
9 online at <http://www.cesm.ucar.edu/models/ccsm3.0/pop>, 2002.

10 Stocker, T. F. and Johnsen, S. J.: A minimum thermodynamic model for the bipolar
11 seesaw. *Paleoceanography*, 18, doi:10.1029/2003PA000920, 2003.

12 Timmermann, A., An, S.-I., Krebs, U. and Goosse, H.: ENSO suppression due to weakening of
13 the north Atlantic thermohaline circulation. *J. Climate*, 18, pp. 3122–3139, doi:
14 10.1175/JCLI3495.1, 2005.

15 Timmermann, A., Okumura, Y., An, S. -I., Clement, A., Dong, B., Guilyardi, E., Hu, A.,
16 Junglaus, J., H., Renold, M., Stocker, T. F., Stouffer, R. J., Sutton, R., Xie, S. -P. and
17 Yin, J.: The Influence of a Weakening of the Atlantic Meridional Overturning
18 Circulation on ENSO. *J. Climate*, 20 (19), pp. 4899-4919. doi:
19 10.1175/JCLI4283.1, 2007a.

20 Timmermann, A., Lorenz, S. J., An, S. -I., Clement, A. and Xie, S. -P.: The effect of orbital
21 forcing on the mean climate and variability of the tropical Pacific. *J. Climate*, 20 (16), pp.
22 4147-4159, doi: 10.1175/JCLI4240.1, 2007b.

23 Tofalo, O., Orgeira, M. J., Compagnucci, R., Alonso, M. S and Ramos, A.:
24 Characterization of a loess-lapeosols section including a new record of the last
25 interglacial stage in Pampean plain, Argentina. *J. S. Am. Earth Sci.*, 31 (1),
26 pp. 81-92, 2011.

27 Turney, C. S. M. and Jones, R. T.: Does the Agulhas Current amplify global
28 temperatures during super-interglacials? *J. Quaternary Sci.*, 25, pp. 839–843, 2010.

29 Yeager, S.G., Shields, C.A., Large, W.G. and Hack, J.J: The low-resolution CCSM3.
30 *J. Climate*, 19, pp. 2545-2566, 2006.

- 1 Wang, B. and Fan, Z.: Choice of South Asian summer monsoon indices. *B. Am.*
2 *Meteorol. Soc.*, 80, pp. 629-638, 1999.
- 3 Wang, Y., Cheng, H., Edwards, R.L., Kong, X., Shao, X., Chen, S., Wu, J., Jiang, X., Wang, X.
4 and An, Z.: Millennial and orbital scale changes in the East Asian monsoon over
5 the past 224,000 years. *Nature*, 451, pp. 1090-1093, 2008.
- 6 Xiao, J. L., An, Z. S., Liu, T. S., Inouchi, Y., Kumai, H., Yosihikawa, S. and Kondo, Y.: East
7 Asian monsoon variation during the last 130,000 years evidence from the Loess Plateau
8 of central China and Lake Biwa of Japan. *Quaternary Sci. Rev.*, 18, pp. 147-157, 1999.
- 9 Yin, Q. Z.: Insolation-induced mid-Brunhes transition in Southern Ocean ventilation and deep-
10 ocean temperature. *Nature*, DOI:10.1038/nature11790, 2013.
- 11 Yin, Q. Z., Berger, A., Driesschaert, E., Goose, H., Loutre, M. -F. and Crusifix, M.: The
12 Eurasian ice sheet reinforces the East Asian summer monsoon during the interglacial
13 500 000 years ago. *Clim. Past*, 4, pp. 79-90, 2008.
- 14 Yin, Q. Z. and Berger, A.: Insolation and CO₂ contribution to the interglacial climate before
15 and after the Mid-Brunhes Event. *Nature Geosci.*, 3, pp. 243-246, 2010.
- 16 Yin, Q. Z. and Berger, A.: Individual contribution of insolation and CO₂ to the interglacial
17 climates of the past 800,000 years. *Clim. Dynam.*, 38 (3-4), pp. 709-724, 2012.
- 18 Zeng, Z. and Guo, Q.: The relationship between the summer precipitation over Asia- Africa
19 monsoon regions and the tropical easterly jet stream. *Chinese Journal of Atmosphere*
20 *Science*, 6, pp. 283–292, 1982.
- 21 Zhao, J. -X., Xia, Q. and Collerson, K, D.: Timing and duration of the Last Interglacial
22 inferred from high resolution U-series chronology of stalagmite growth in Southern
23 Hemisphere. *Earth Planet. Sc. Lett.*, 184, issues 3-4, pp. 635-644, 2001.

24
25
26
27
28
29
30

Table 1. Greenhouse gas concentrations and astronomical parameters used for the PI and the last interglacial simulations in both LOVECLIM and CCSM3.

date (kaBP)	Greenhouse gases				Astronomical parameters		
	CO2 (ppmv)	CH4 (ppbv)	N2O (ppbv)	CO2eq (ppmv)	eccentricity	obliquity (deg)	longitude perihelion (deg)
0	280	760	270	280	0.01672	23.446	102.04
127	287	724	262	284	0.03938	24.04	275.41

Table 2. Global mean surface temperature (°C) of MIS-5e and PI in CCSM3 and LOVECLIM. DJF and JJA stand for December-January-February and June-July-August, respectively.

	Annual		DJF		JJA	
	CCSM3	LOVECLIM	CCSM3	LOVECLIM	CCSM3	LOVECLIM
MIS5	12.3	16.5	9.6	13.7	15.0	19.7
PI	12.5	16.0	10.8	14.1	14.1	18.2
anomaly	-0.2	0.5	-1.2	-0.4	0.9	1.4

Table 3. Reconstructed surface temperature anomaly (difference between MIS-5e and PI) based on proxy records and the corresponding simulated anomaly by CCSM3 and LOVECLIM.

Study	Coordinates/area	Delta T °C	CCSM3 °C	LOVECLIM °C
JJA				
Andersen et al (2004)	42.32W; 75.10N	5	3.8	6.3
Andreev et al. (2004)	141E; 73N	4-5	1.6	2.3
Beaulieu and Reille (1992)	6.5E; 47.73N	1.7	4.6	3.4
Hahne et al. (1994)	7.57E, 52.4N	1.4	2.6	2.7
Labeyrie et al. (1996)	96.28E; 46S	3 and more	-0.07	0.4
Lozkhin and Anderson (1995)	132-180E; 60-70N	4-8	2.9	1.8
Mamakowa (1989)	~16.57E; ~50.88N	2.5	4.6	3.7
Muhs et al. (2001)	148-164W; 58-66N	0-2	0.4	2.1
Otto-Bliesner et al. (2006a); model study	0-360E; 60-90N	2.4	2.2	3
Pahnke et al. (2005)	174.55E; 45.3S	~ 2	-0.01	0.2
DJF				
Bianchi and Gersonde (2002)	40E-35W; 52-59S	2-3.5	0.2	0.6
Crosta et al. (2004)	160E; 55S	5-6	0.1	0.2
Lozkhin and Anderson (1995)	132-180E; 60-70N	4	-0.6	3.7
	0-360E; 50S-60S		-0.1	0.7
Annual				
EPICA (Jouzel et al., 2007)	123E; 75S	2-4	-0.2	0.8
Vostok (Petit et al., 1999)	106E, 78S	2.3	-0.1	0.8
	0-360E; 60S-90S		-0.2	1.7
	0-360E; 70S-90S		-0.2	1.5

Table 4. Precipitation anomalies (mm/day, MIS-5e minus PI) over East Asia (20°N-40°N; 95°E-145°E), India (6.5°N-37.5°N; 67.5°E-101.5°E) and Africa (0-30°N; 15°W-45°E), simulated by CCSM3 and LOVECLIM.

	CCSM3	LOVECLIM
East Asia	-0.4	0.4
India	0.75	2.05
Africa	1.7	3.2

Figure captions

Figure 1. Difference in the latitudinal-seasonal insolation distribution (Wm^{-2}) between 127ka BP and PI. The true longitudes 0° and 180° correspond to the spring and fall equinoxes, respectively; 90° and 270° are for the summer and winter solstices, respectively.

Figure 2. JJA surface temperature ($^\circ\text{C}$) anomaly (MIS-5e minus PI) simulated by a) CCSM3 and b) LOVECLIM. Temperature anomaly between black and grey dashed lines is statistically insignificant.

Figure 3. JJA sea-ice fraction (%) anomaly simulated by a) CCSM3 and b) LOVECLIM.

Figure 4. DJF surface temperature ($^\circ\text{C}$) anomaly simulated by a) CCSM3 and b) LOVECLIM. Temperature anomaly between black and grey dashed lines is statistically insignificant.

Figure 5. DJF sea-ice fraction (%) anomaly simulated by a) CCSM3 and b) LOVECLIM.

Figure 6. Annual surface temperature ($^\circ\text{C}$) anomaly simulated by a) CCSM3 and b) LOVECLIM. Temperature anomaly between black and grey dashed lines is statistically insignificant.

Figure 7. JJA precipitation (mm/day) anomalies simulated by a) CCSM3 and b) LOVECLIM. Precipitation anomaly between black and grey dashed lines is statistically insignificant.

Figure 8. JJA surface wind (m/s) anomaly for region 10°S - 40°N and 0 - 160°E in a) CCSM3 and b) LOVECLIM.

Figure 9. Tropical Easterly Jet (m/s) anomaly at 200hPa (10°S - 50°N and 0 - 160°E) in a) CCSM3 and b) LOVECLIM.

Figure 10. Vertical velocity (Pa/s) anomaly at 400mb for region 0 - 40°N and 0 - 360°E , simulated in CCSM3.

Figure 11. Indian Monsoon Index anomaly (MIS-5e minus PI) in CCSM3.

Figure 12. DJF precipitation (mm/day) anomaly simulated by a) CCSM3 and b) LOVECLIM. Precipitation anomaly between black and grey dashed lines is statistically insignificant.

Figure 13. Vegetation fraction (%) simulated by BIOME4 for a) trees, b) grass, c) desert and by LOVECLIM for d) trees, e) grass, f) desert.

Figure 14. CCSM3 and LOVECLIM simulations averaged over 5°S - 5°N between 150 - 275°E of a) SST ($^\circ\text{C}$), b) wind stress (Pa) and c) depth of the thermocline (m).

Figure 15. CCSM3 and LOVECLIM results averaged over NINO3.4 region (5°S - 5°N and 190 - 240°E) for a) spectrum for SST anomalies, b) monthly standard deviation for SST anomalies and c) monthly SST anomalies.

Figure 1

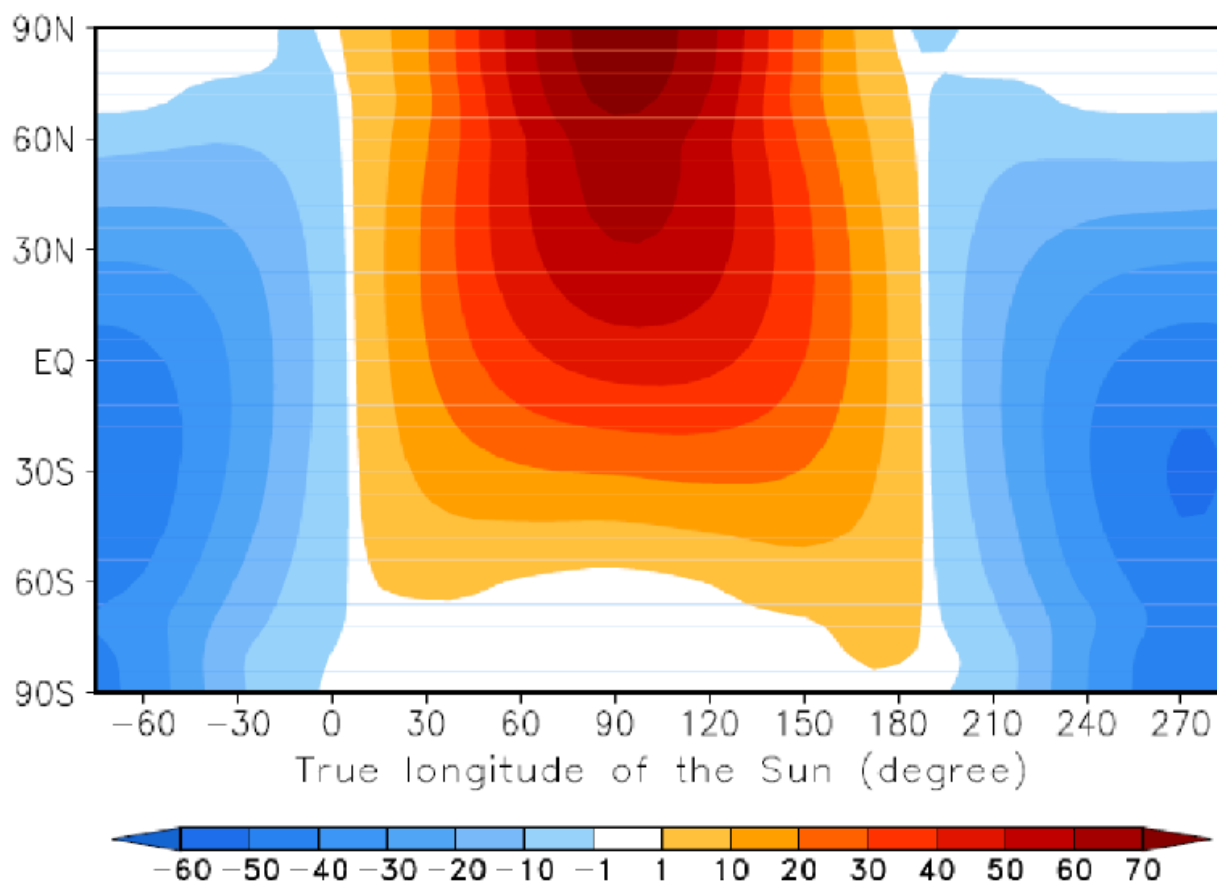


Figure 2

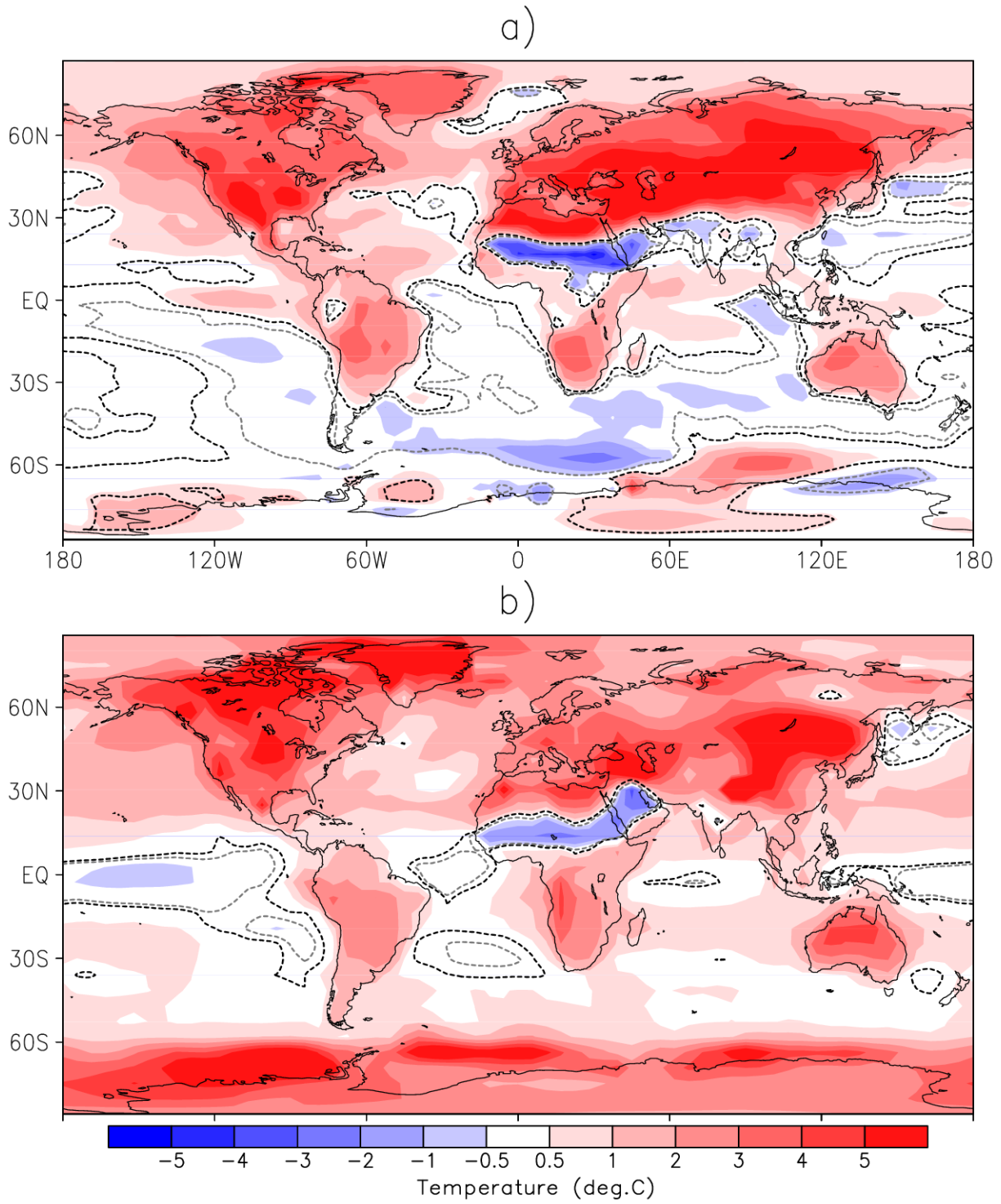


Figure 3

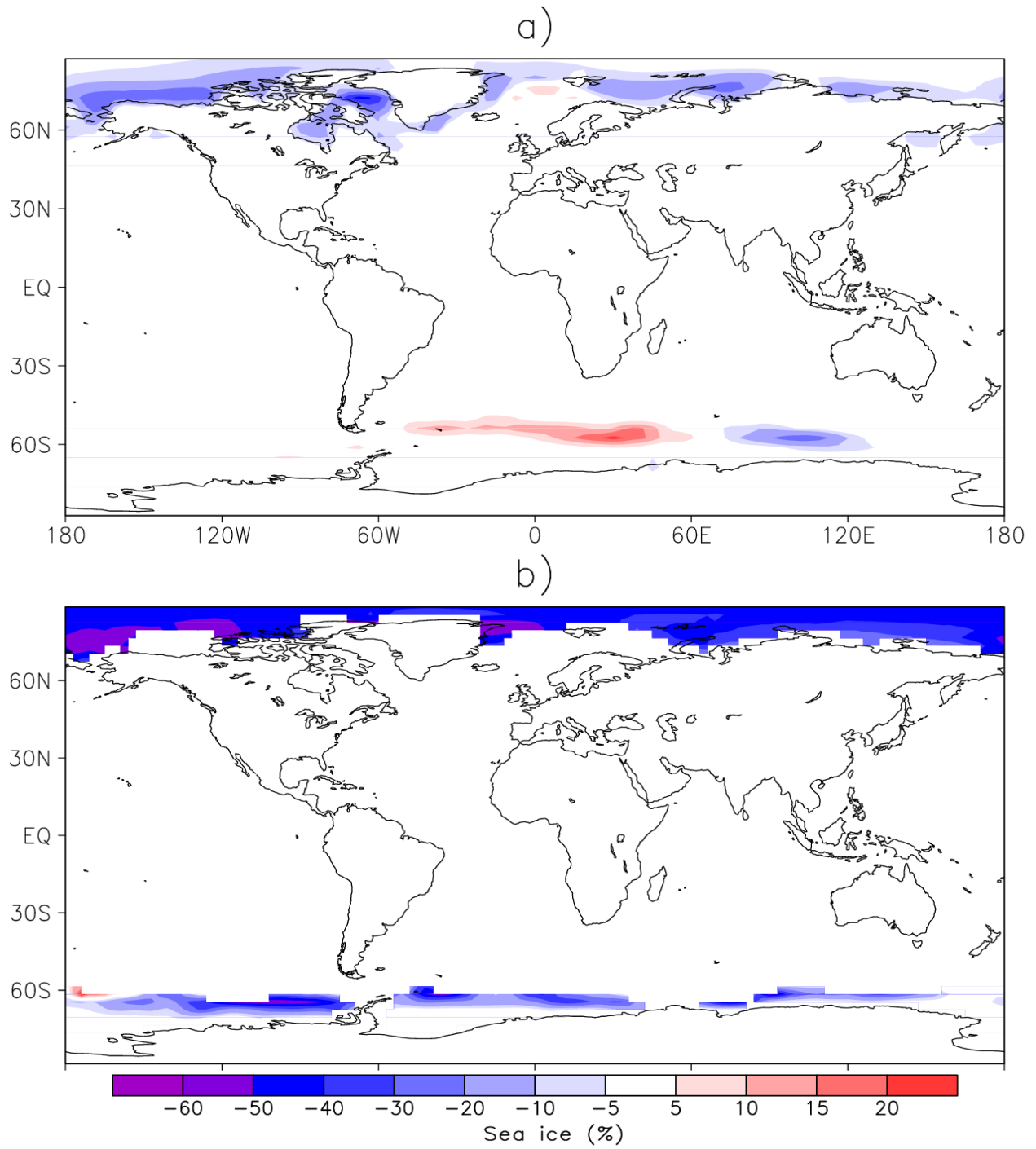


Figure 4

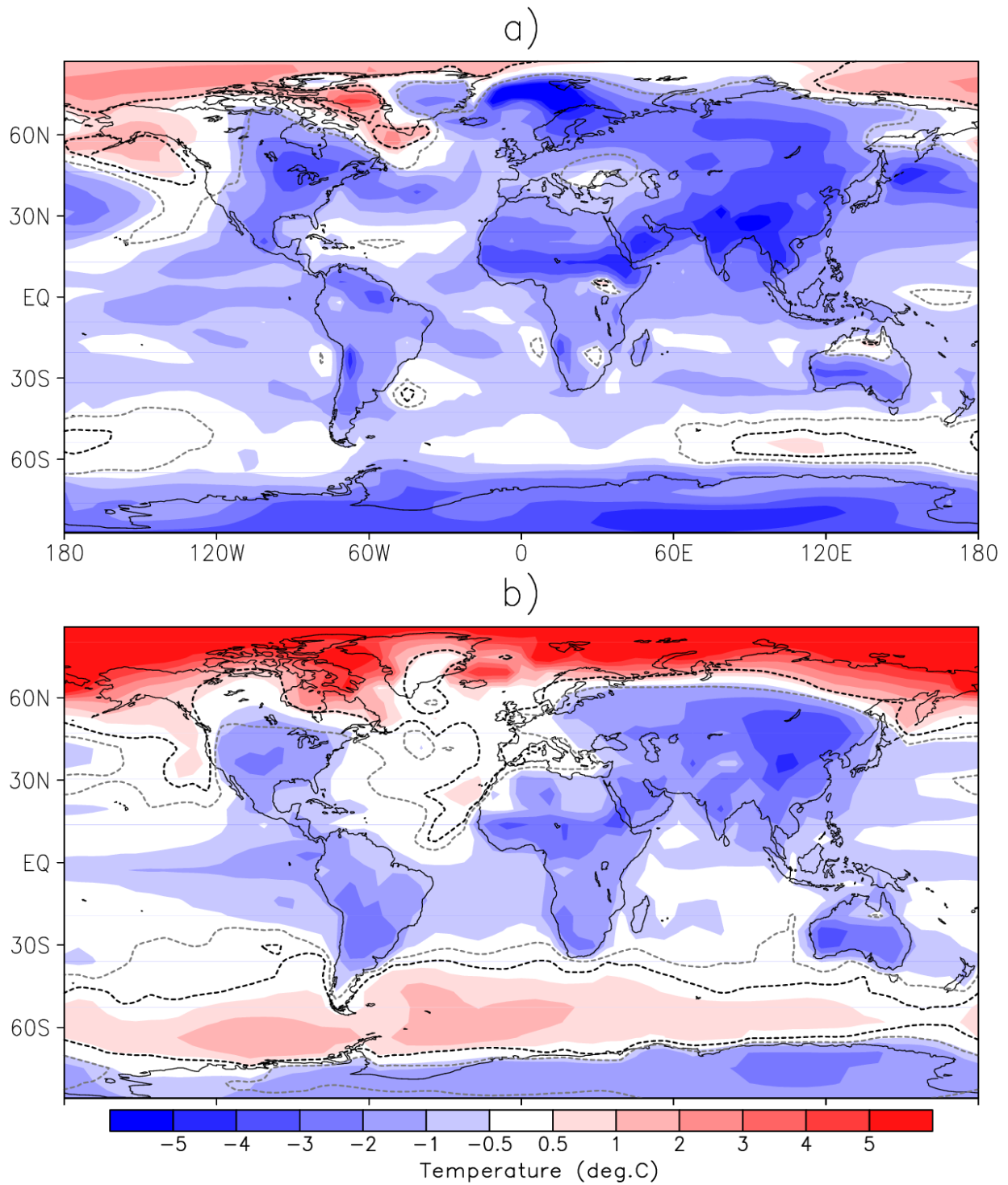


Figure 5

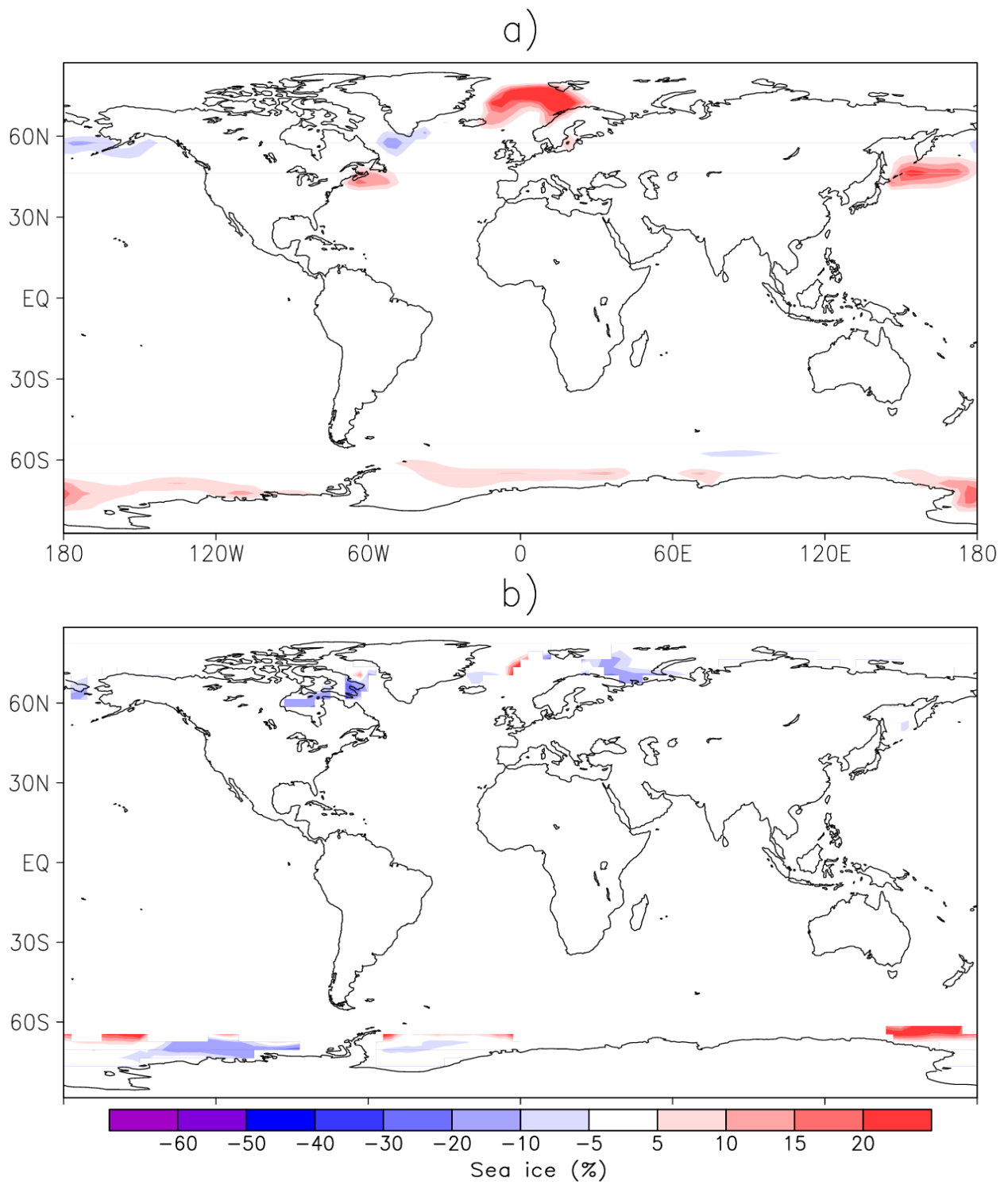


Figure 6

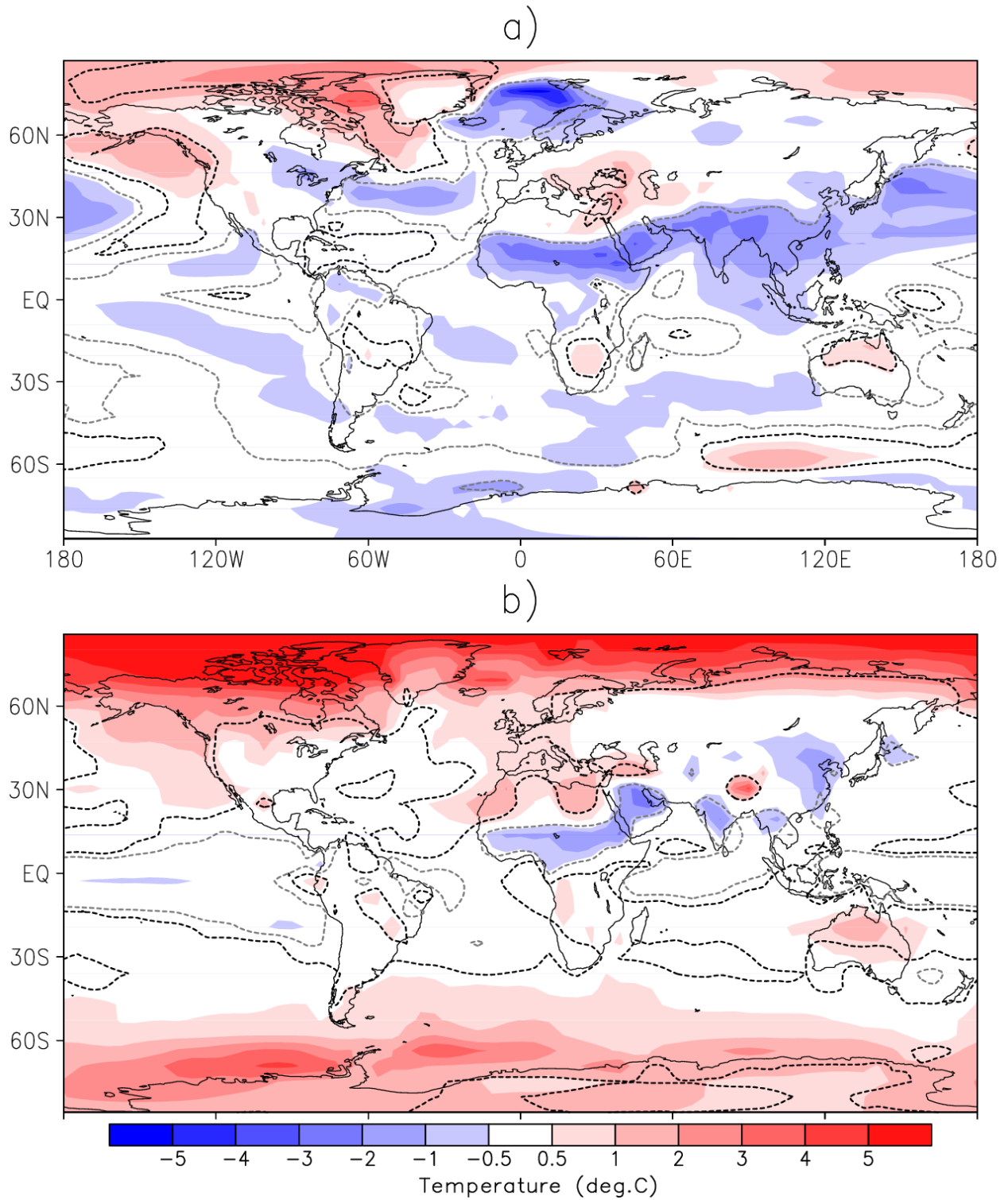


Figure 7

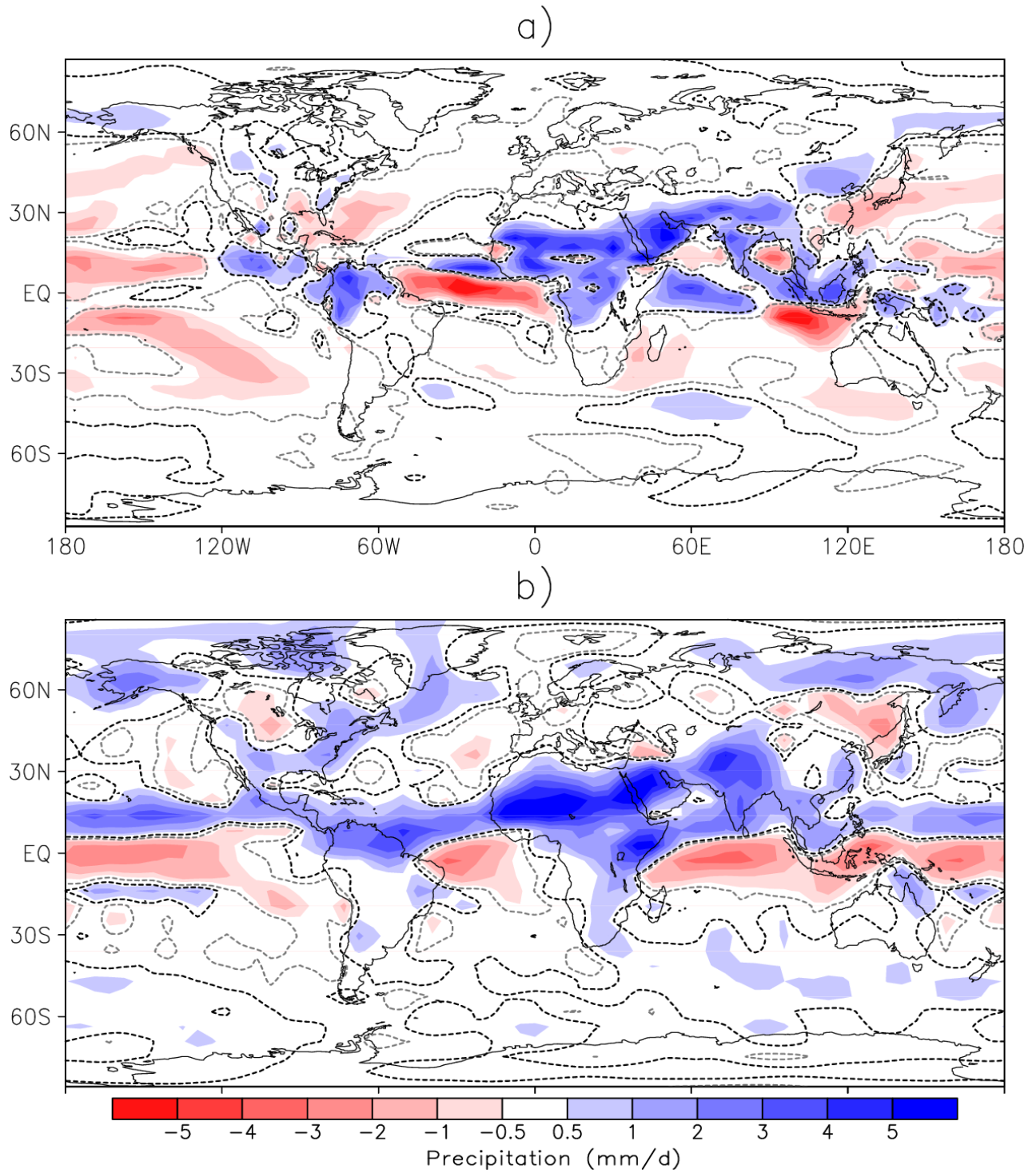


Figure 8

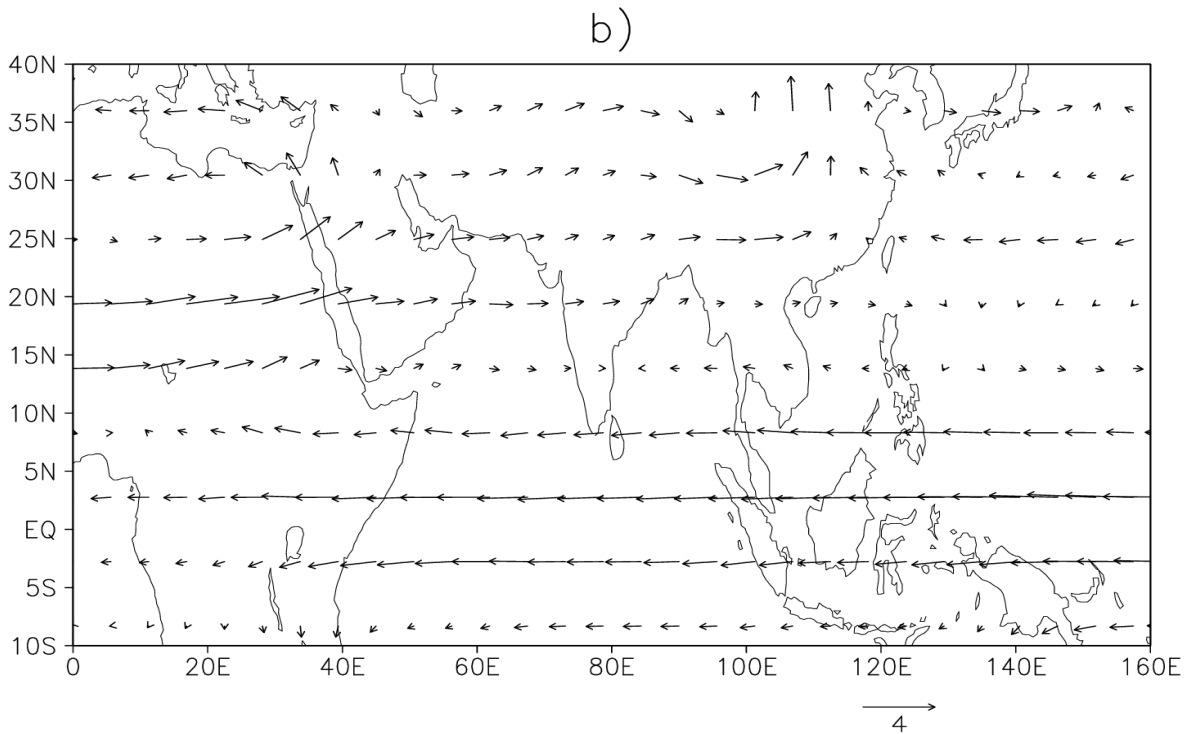
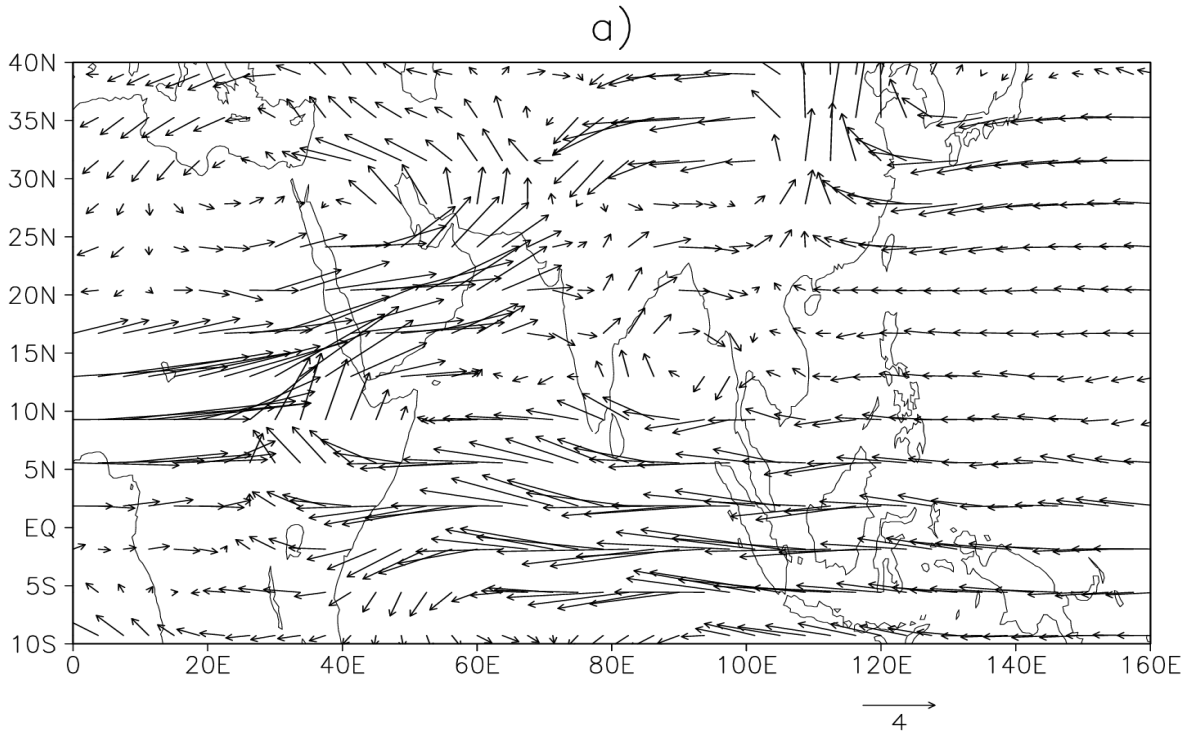


Figure 9

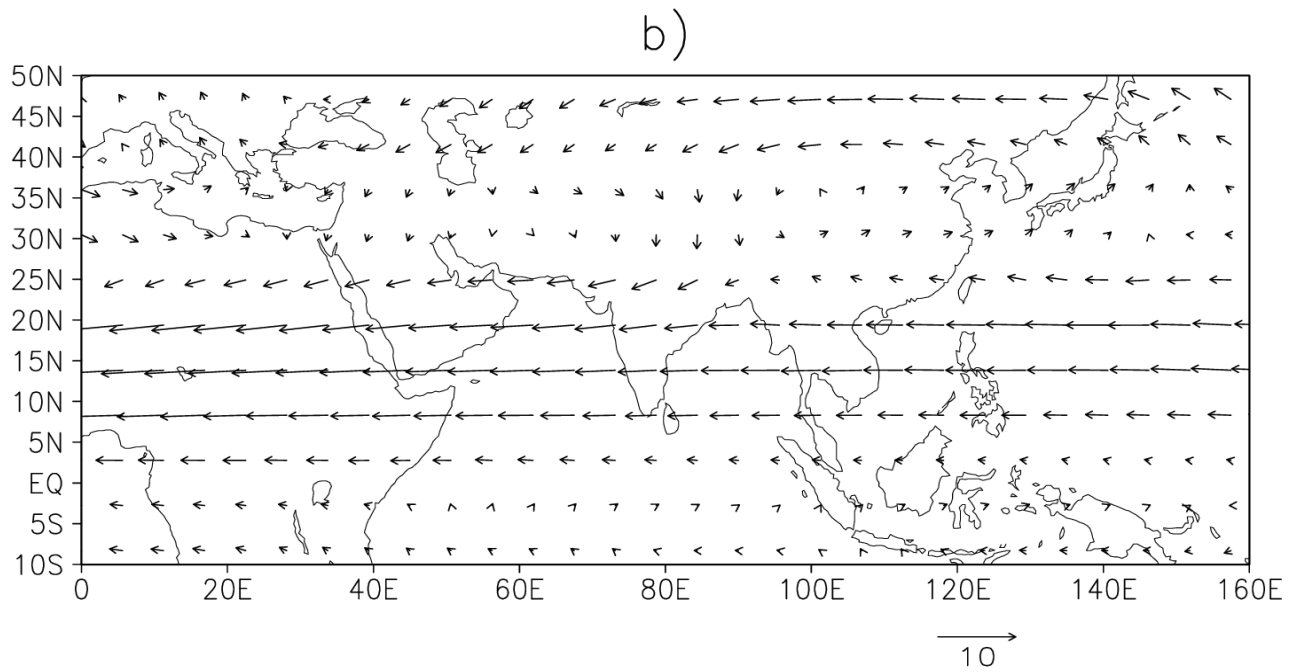
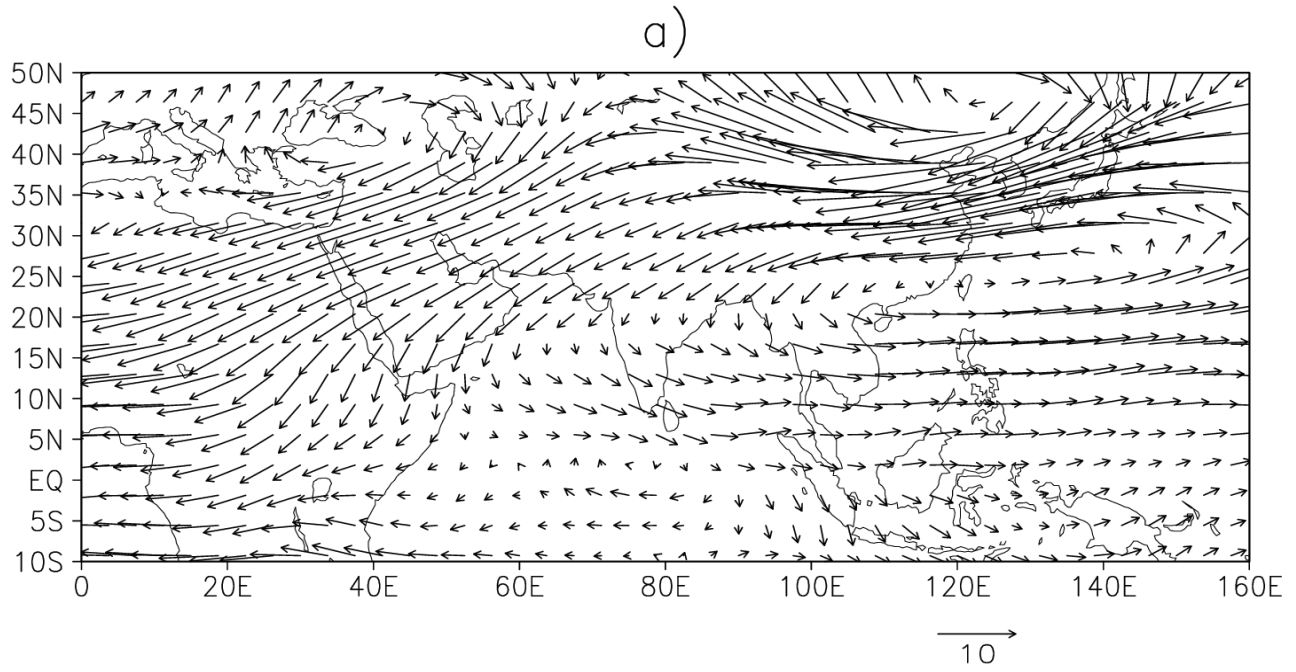


Figure 10

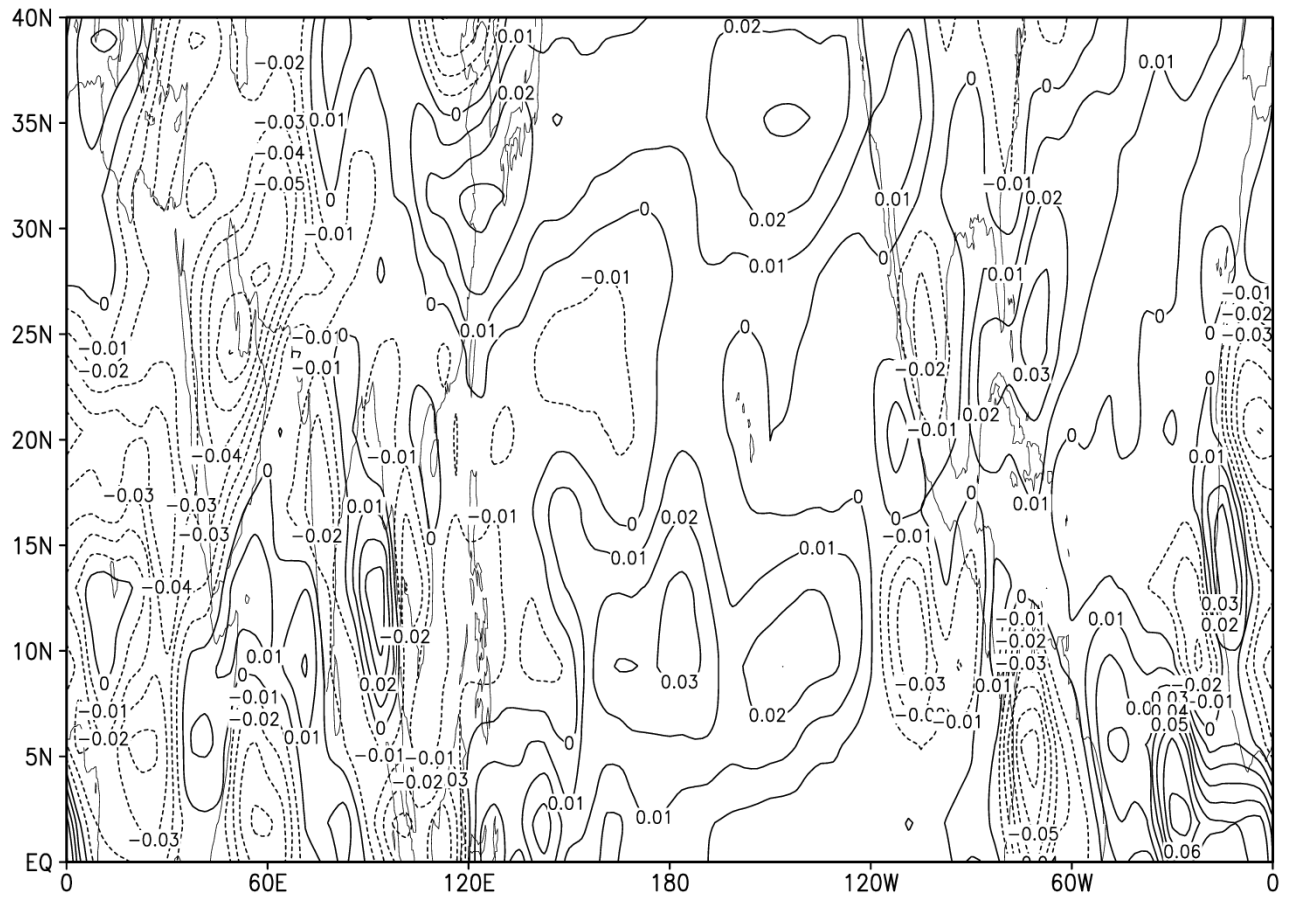


Figure 11

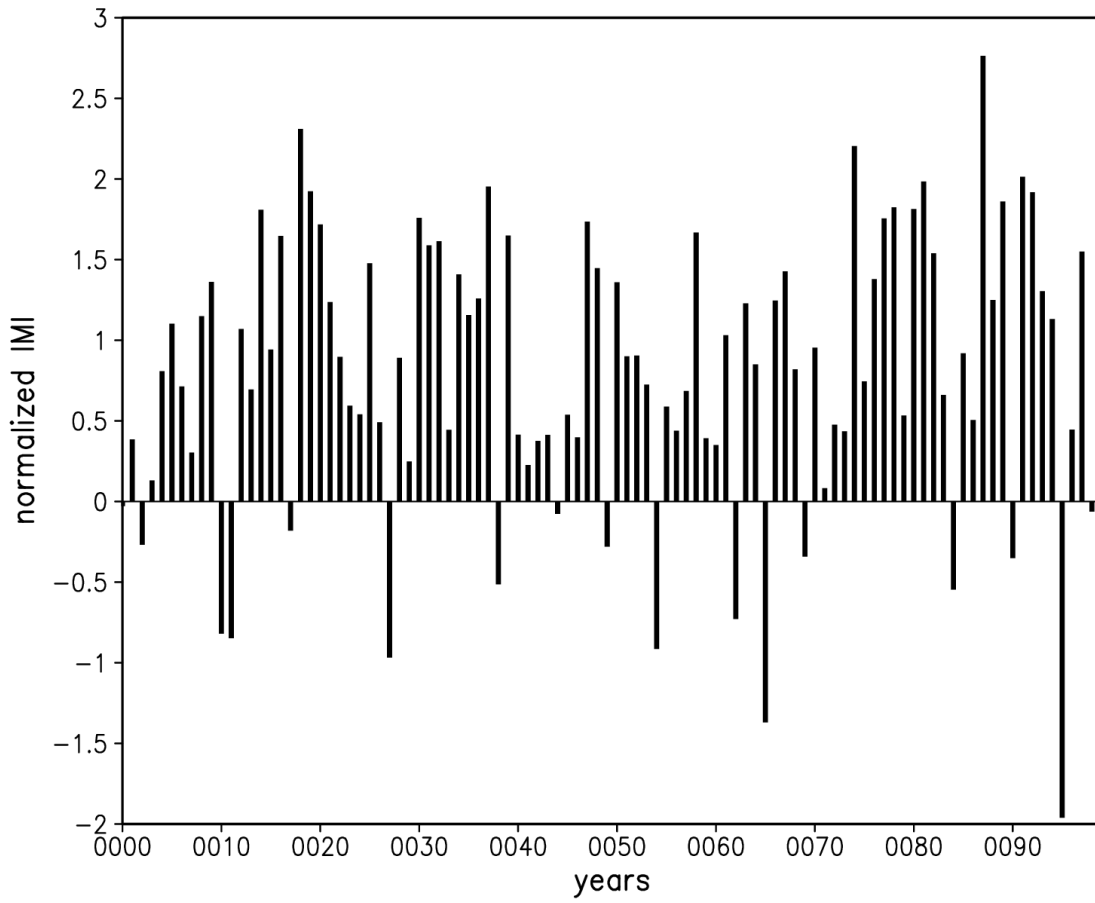


Figure 12

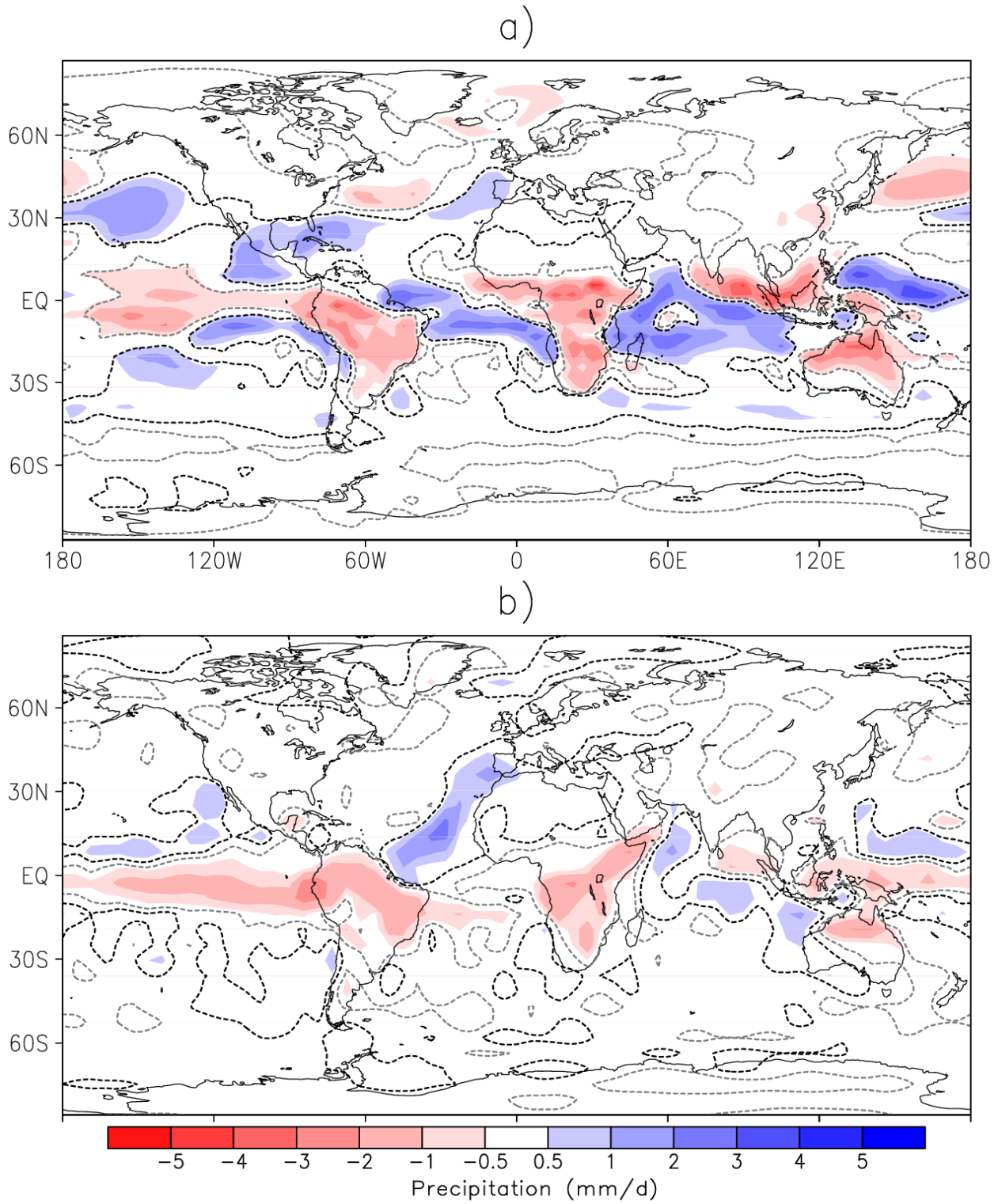


Figure 13

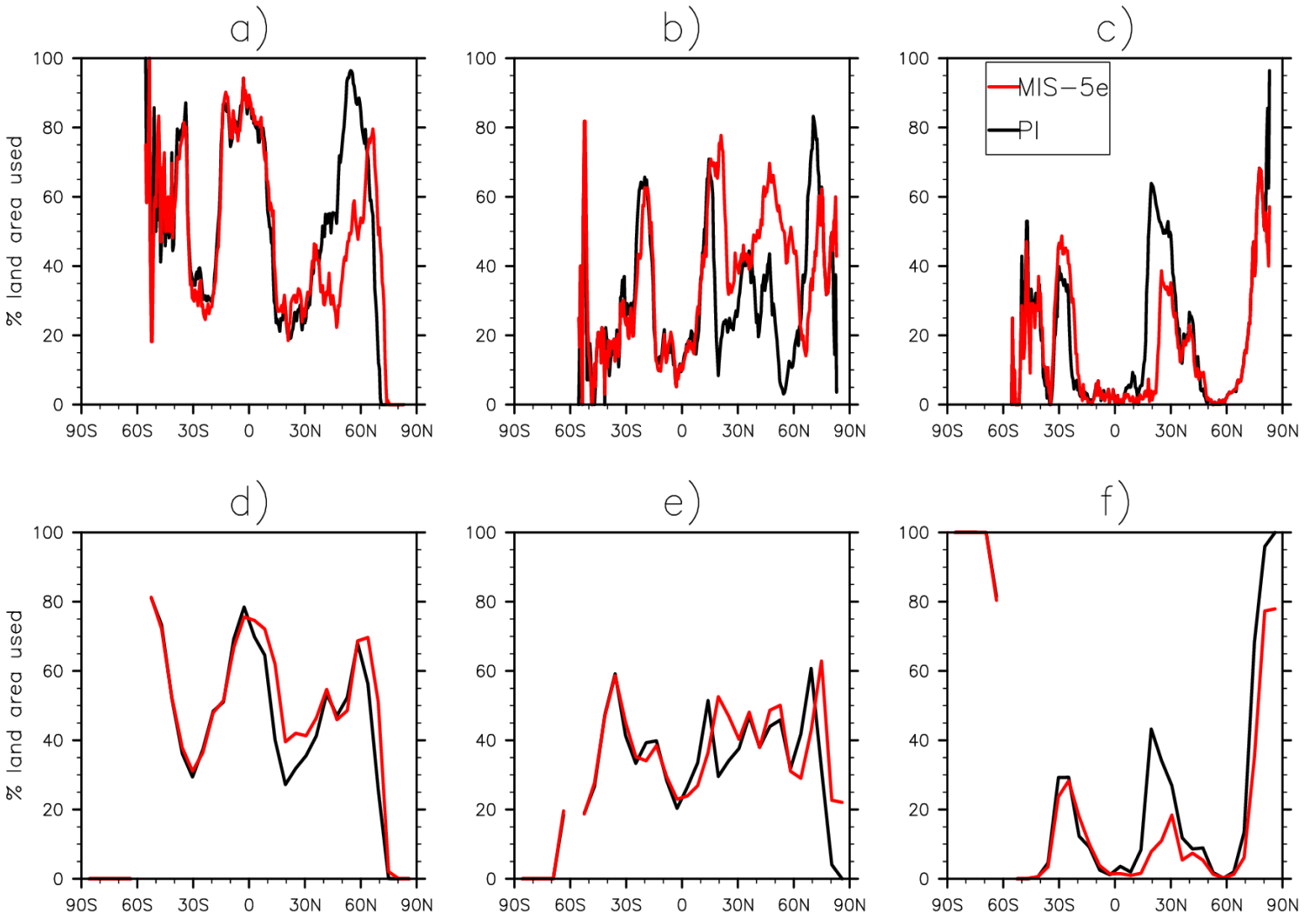


Figure 14

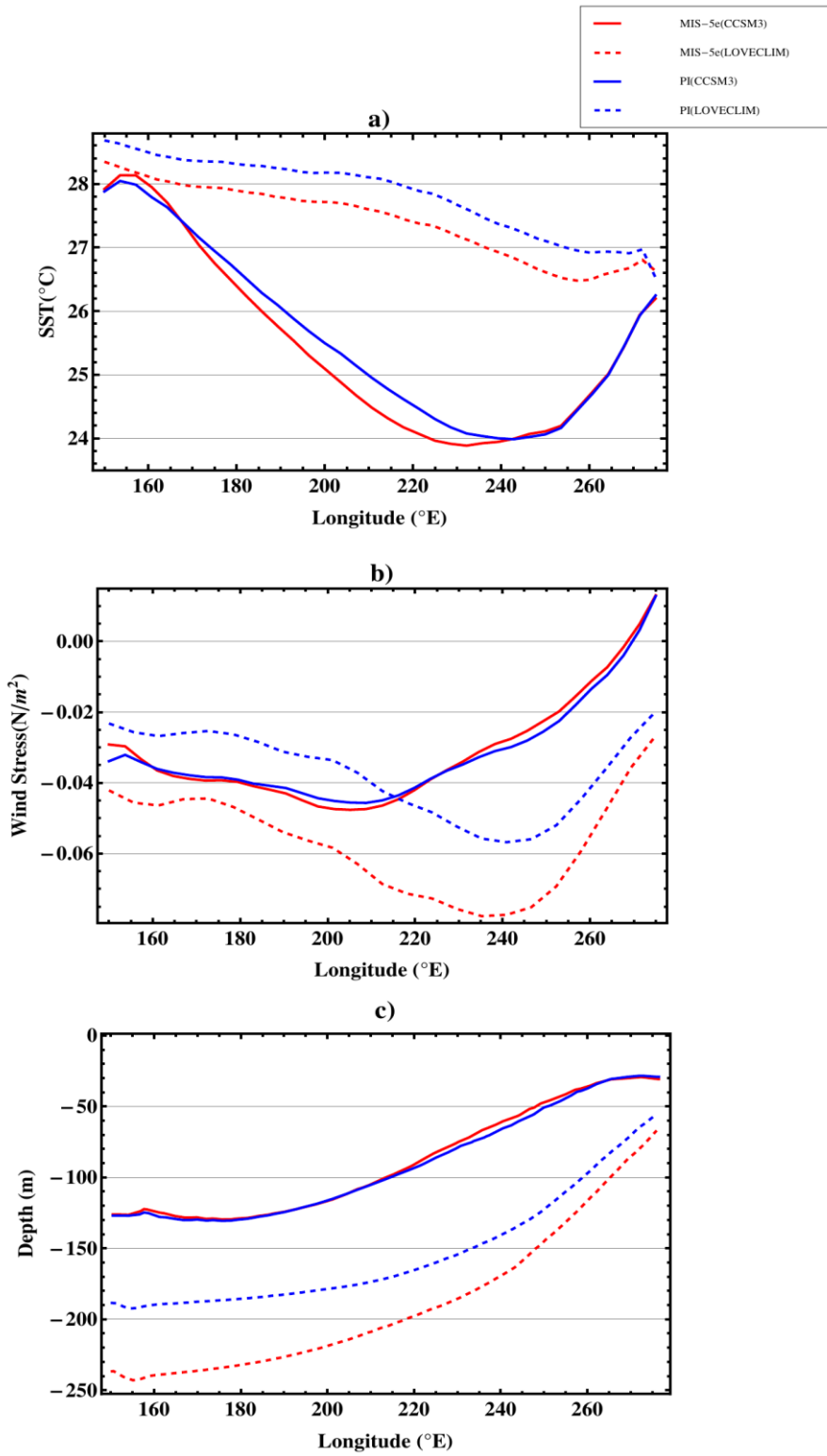


Figure 15

